

UC Berkeley

UC Berkeley Previously Published Works

Title

Scanning electrochemical probe microscopy investigation of two-dimensional materials

Permalink

<https://escholarship.org/uc/item/9w5995ft>

Journal

2D Materials, 11(3)

ISSN

2053-1583

Authors

Adanigbo, Pelumi

Romo-Jimenez, Jorge

Zhang, Kaidi

et al.

Publication Date

2024-07-01

DOI

10.1088/2053-1583/ad4e45

Copyright Information

This work is made available under the terms of a Creative Commons Attribution License, available at <https://creativecommons.org/licenses/by/4.0/>

Peer reviewed

TOPICAL REVIEW • OPEN ACCESS

Scanning electrochemical probe microscopy investigation of two-dimensional materials

To cite this article: Pelumi Adanigbo *et al* 2024 *2D Mater.* 11 032001

View the [article online](#) for updates and enhancements.

You may also like

- [Establishing the morphotropic phase boundary in van der Waals ferroelectrics](#)
Jianming Deng, Zhengqian Fu, Yixuan Zhang *et al.*
- [Electrochemical Charge Storage Properties of Vertically Aligned Carbon Nanotube Films: The Activation-Enhanced Length Effect](#)
Billyde Brown, Charles B. Parker, Brian R. Stoner *et al.*
- [Dopant Redistribution and Activation in Ga Ion-Implanted High Ge Content SiGe by Explosive Crystallization during UV Nanosecond Pulsed Laser Annealing](#)
Toshiyuki Tabata, Huet Karim, Fabien Rozé *et al.*



TOPICAL REVIEW

OPEN ACCESS

RECEIVED
6 March 2024REVISED
6 May 2024ACCEPTED FOR PUBLICATION
21 May 2024PUBLISHED
4 June 2024

Original content from this work may be used under the terms of the [Creative Commons Attribution 4.0 licence](#).

Any further distribution of this work must maintain attribution to the author(s) and the title of the work, journal citation and DOI.



Scanning electrochemical probe microscopy investigation of two-dimensional materials

Pelumi Adanigbo¹, Jorge Romo-Jimenez¹, Kaidi Zhang² , Sonal Maroo², Kwabena Bediako^{2,3} and Yun Yu^{1,4,*}

¹ Department of Chemistry and Biochemistry, George Mason University, Fairfax, VA 22030, United States of America

² Department of Chemistry, University of California, Berkeley, CA 94720, United States of America

³ Chemical Sciences Division, Lawrence Berkeley National Laboratory, Berkeley, CA 94720, United States of America

⁴ Quantum Science and Engineering Center, George Mason University, Fairfax, VA 22030, United States of America

* Author to whom any correspondence should be addressed.

E-mail: yyu26@gmu.edu

Keywords: SECM, SECCM, electrochemistry

Abstract

Research interests in two-dimensional (2D) materials have seen exponential growth owing to their unique and fascinating properties. The highly exposed lattice planes coupled with tunable electronic states of 2D materials have created manifold opportunities in the design of new platforms for energy conversion and sensing applications. Still, challenges in understanding the electrochemical (EC) characteristics of these materials arise from the complexity of both intrinsic and extrinsic heterogeneities that can obscure structure–activity correlations. Scanning EC probe microscopic investigations offer unique benefits in disclosing local EC reactivities at the nanoscale level that are otherwise inaccessible with macroscale methods. This review summarizes recent progress in applying techniques of scanning EC microscopy (SECM) and scanning EC cell microscopy (SECCM) to obtain distinctive insights into the fundamentals of 2D electrodes. We showcase the capabilities of EC microscopies in addressing the roles of defects, thickness, environments, strain, phase, stacking, and many other aspects in the heterogeneous electron transfer, ion transport, electrocatalysis, and photoelectrochemistry of representative 2D materials and their derivatives. Perspectives for the advantages, challenges, and future opportunities of scanning EC probe microscopy investigation of 2D structures are discussed.

1. Introduction

The discovery and development of atomically thin crystals (so-called two-dimensional, 2D, materials) has been a breakthrough for material science. Isolating single/few atomic layers from bulk layered materials has led to the discovery of a wide range of exotic phenomena [1, 2]. Interests in exploring the fascinating behavior of 2D materials have seen rapid growth across multiple disciplines including electronics [3, 4], mechanics [5], photonics [6], and chemistry [7, 8]. Two-dimensional (2D) materials have shown great promise in supporting the interconversion of electrical energy and chemical energy due to their large surface area-to-volume ratio and highly tunable physicochemical properties [8].

Further development of 2D materials in the field of electrochemistry will rely on a deeper understanding of the fundamental factors that underpin interfacial charge transfer and chemical reactivity associated with these physicochemical properties. Importantly, heterogeneity arising from the presence of structural modifications and defects of the 2D crystals plays a significant role in determining the material's overall electrochemical (EC) behavior. Advanced characterization of the EC behavior of any 2D material, and mechanistic insights into the structure–function relationship of these systems is vital for identifying appropriate fundamental and/or engineering strategies that may optimize the system's potential in energy conversion and storage applications.

Several advanced techniques have been developed to characterize the properties of 2D materials that are critical for their EC performance. For instance, detailed morphology and crystal orientation of 2D flakes can be readily visualized by high-resolution transmission electron microscopy combined with electron diffraction [9, 10]. X-ray characterization techniques such as x-ray absorption spectroscopy can provide quantitative structural information such as the oxidation state, coordination number and interatomic distances [11, 12]. Raman spectroscopy is especially powerful in probing the evolution of structure and surface chemistry of 2D materials due to its sensitivity to the layer number, defects, strain, and doping level [13–15]. However, with regard to EC characterization, conventional electroanalytical techniques suffer from their inability to isolate or resolve the contributions of heterogeneities at electrode surfaces. An alternative EC testing platform involves the fabrication of individual 2D flakes into on-chip devices [16, 17], where local measurement may be performed by selectively exposing 2D flakes using lithography. This approach has provided a more direct strategy to spatially resolve EC activity and identify potential active sites. However, the dimensions of on-chip devices in the current stage are limited to micrometer scales, while higher spatial resolution is required to reveal the behaviors of (sub)nanoscale heterogeneities, which may include atomic defects and step edges. The throughput of this technique is also limited by the fact that only a small portion of the 2D material can be probed at a time.

Scanning electrochemical microscopy (SECM) is an electroanalytical scanning probe technique capable of obtaining the EC activity map of a sample with high spatial resolution. Engstrom pioneered the technique by employing ultramicroelectrodes to map concentration profiles within the diffusion layer at a macroelectrode surface [18]. This technique was later introduced as SECM by Bard [19]. In an SECM experiment, an ultramicroelectrode is scanned over the sample to build an EC map that depends on both the topography and the EC activity of the substrate. Scanning electrochemical cell microscopy (SECCM) was derived from SECM and introduced by Unwin in 2010 [20, 21]. In an SECCM experiment, an electrolyte-filled nanopipette is brought into contact with the sample to form a miniaturized liquid cell and perform localized EC measurements. Both techniques are suitable for carrying out spatially resolved, localized EC characterization with their resolution defined by the probe size. The success of applying scanning EC probe techniques for localized measurement stems from the exceptional spatial resolution realized by miniaturization of the EC probes (i.e. nanoelectrodes or nanopipette) that may attain spatial resolutions ≤ 10 nm [22, 23]. Shrinking the physical size of the probes down

to the nanometer range also permits steady-state response readily attained at the nanogap/nanocell. Well-established theories in combination with finite-element simulations for various regimes of measurements have granted SECM/SECCM the capabilities to quantitatively interpret the EC data [22, 24].

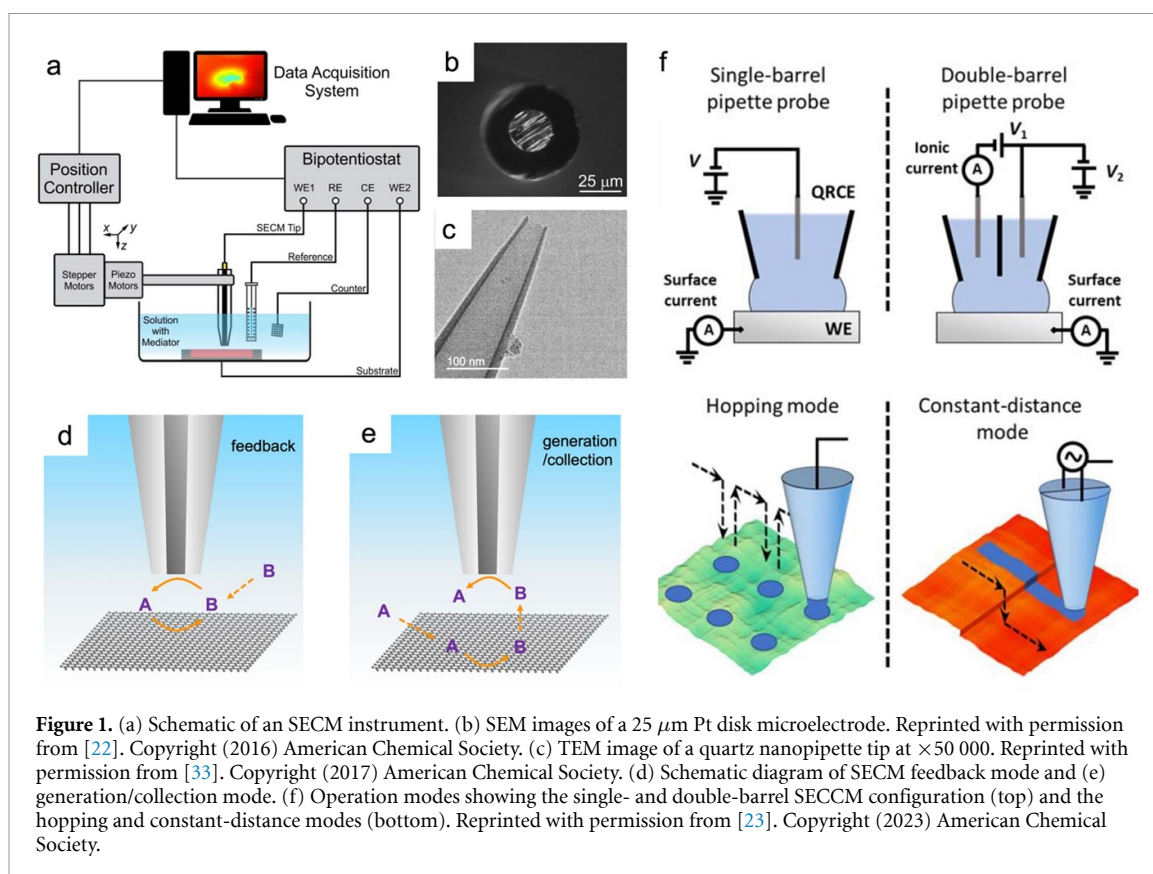
In comparison with many widely employed material characterization techniques, SECM/SECCM are uniquely fitted to provide direct insights into the EC behavior of the samples at the nanoscale level. In this context, scanning EC probe techniques are of increasing interest as platforms to investigate interfacial charge transfer at 2D material electrodes [25, 26]. The effects of structural heterogeneities (e.g. step edges, terraces, stacking variants) as well as external engineering (e.g. defects, substrate, strain) on the electron transfer kinetics and electrocatalytic activities have been clearly revealed with these spatially resolved EC characterization approaches. In this review, we present the basic principles of the SECMs, followed by a comprehensive summary of the present state-of-the-art SECM/SECCM work on 2D materials covering their research background, key data, and valuable insights obtained from the study. Finally, we discuss the current challenges and limitations of these methods, and signpost new avenues and future opportunities in the development of scanning EC probe microscopy to understand the chemistry of 2D materials.

2. Principles of SECM and SECCM

In this section we provide a concise overview of the working principles of SECM/SECCM. While this review places an emphasis on the studies of 2D materials, the readers are encouraged to refer to many comprehensive reviews of scanning EC probe methods [21–23, 27–30] applied in a wide range of disciplines.

2.1. SECM

A schematic of a typical SECM instrument is shown in figure 1(a). The positioning system generally consists of three-dimensional stepper motors coupled with piezoelectric actuators for precise positioning of the probe relative to the substrate. A low current bipotentiostat is used to independently modulate and measure the potential and the current at the probe and substrate, respectively. A data acquisition and a control system are required to synchronize data and coordinate the bipotentiostat and the positioning system. An SECM probe (generally referred to as an SECM tip) is a critical component that defines the spatial resolution of the measurement. While a substantial number of reports have focused on the design and fabrication of various types of probes [31–33], disk-shaped micro(nano)electrodes are generally the most common geometry (figure 1(b)). Other important accessories of an SECM include EC cells, vibration



isolation stages, optical microscopes, and complementary spectrometers [22].

2.1.1. Modes of operation

In an SECM experiment, the scanning of the tip over the substrate surface is generally operated in two complementary modes. In the feedback mode experiment (figure 1(d)), the SECM tip is brought within a short distance (comparable to the probe size) of the substrate surface. With a suitable electrical potential applied to the tip, the redox active reactant (B) is oxidized/reduced to the product (A) at the tip surface. The regeneration of B at an electroactive substrate and the redox cycling of A/B within the tip-substrate gap result in an increasing tip current with decreasing distance (positive feedback). If the substrate is inert, the tip current decreases with decreasing distance due to the hindered diffusion of B to the tip electrode (negative feedback). The measurement of the current response as a function of the tip-to-substrate distance (generally referred to as an ‘approach curve’) has a strong dependence on the apparent reaction kinetics at the substrate. The approach curve can be described using analytical approximations [34, 35] that allow charge transfer kinetics to be extracted quantitatively. The feedback mapping experiments are carried out by raster scanning the tip over the sample while maintaining the tip-substrate distance in the feedback region. The obtained map depends on both the topography and reactivity of the substrate material.

In substrate generation/tip collection mode (SG/TC, figure 1(e)), the tip collects the redox species generated at the substrate surface (e.g. B in figure 1(e)). The collection efficiency depends on the separation distance and relative sizes of the tip and the substrate. A lateral scan of the tip over the surface is used to identify ‘hot spots’ where reactions occur at a higher rate which and thus more products are collected at the tip. Tip generation/substrate collection mode (TG/SC) is operated where the redox species are generated at the tip and subsequently collected by the substrate, and is predominantly used for performing local modification of substrate [36]. In addition to feedback and generation/collection (GC) modes, competition mode has developed for determining surface activities. In this mode, tip and substrate compete for the same redox process, and the consumption of redox species at substrate leads to the decrease in tip current [22]. The attenuation of tip current is then used as an indirect report of the substrate catalytic activity.

The combination of SECM with atomic force microscopy (SECM-AFM) offers a promising approach to correlating EC activities with the nanoscopic topography of a sample [37, 38]. The integration of a nanoelectrode to the apex of an AFM probe allows local EC measurements taken at a controllable distance to the substrate. The ability to independently obtain topographic and EC information permits a reliable evaluation of the EC activity. Similarly, a hybrid system of SECM and scanning ion

conductance microscopy (SICM) has been developed for simultaneous imaging of noncontact topography and local EC species [39, 40]. While this technique is particularly useful for probing soft samples such as living cells, it is not addressed in this review as detailed SICM studies of 2D materials remain few.

2.1.2. Types of reactions

Interfacial EC processes are generally classified as either outer-sphere or inner-sphere redox processes [41, 42]. In outer-sphere redox reactions, there are minimal bonding interactions between the redox species and electrode surface in interfacial electron transfer. These molecules undergo oxidation and reduction reversibly with simple reaction mechanisms. They are ideal mediators used in the feedback mode due to the EC reversibility and fast heterogeneous kinetics to achieve redox cycling between the tip and substrate. Combined with mass transport modeling, the reaction kinetic parameters are readily extracted from the feedback current collected at the tip. These properties are often correlated with the surface conductivity and electronic density of the studied 2D materials.

Inner-sphere redox (catalytic) processes are associated with bonding or adsorption of reactants, intermediates, and/or products to the electrode surface. The reactions involve two or more electrons, multiple elementary steps, and even coupled homogeneous chemical reactions. GC mode is particularly useful in collecting and quantifying intermediates that are otherwise inaccessible with other methods. Competition mode can be employed to indirectly probe the consumption rate of the reactants at the sample. The obtained reactivity is dictated by the ability to stabilize/destabilize key catalytic intermediates of the probed 2D surface.

2.2. SECCM

SECCM was derived from SECM and has developed into a new versatile scanning probe microscopy. The SECCM instrument has similar components to SECM but operates on a distinct principle: direct EC measurement is carried out at the cell formed between the sample and the nanopipette probe.

2.2.1. Dual channel setup

A double barrel (theta) nanopipette was originally used as the SECCM probe [21]. Two quasi-reference counter electrodes (QRCEs) are placed in each channel filled with electrolyte solution (figure 1(f)). The EC cell consists of a meniscus droplet formed at the end of the pipette. A potential (V_1) is applied between the QRCEs to induce an ionic conductance current through the hanging meniscus. The change of ion current upon meniscus contact is detected with high sensitivity, allowing any surface to be probed regardless of its conductivity. The probe moves laterally while the pipette height is adjusted to maintain a constant meniscus shape and resolve

topographical features (constant-distance mode). An additional voltage (V_2) between the substrate and QRCE is applied to implement voltametric and chronoamperometric experiments at the substrate.

2.2.2. Single channel setup

A simpler SECCM configuration based on single barrel nanopipettes (figure 1(c)) has been developed for synchronous EC/topographical imaging with high spatial and temporal resolution [30, 43]. This approach was reported first as scanning micropipet contact method [44] and later renamed single channel SECCM. The QRCE is kept at a desired voltage relative to the conductive substrate so that a measurable current will flow upon meniscus contact with the substrate, which causes the instrument to halt the vertical approach. Imaging is usually operated in a 'hopping mode' where the nanopipette lands onto the substrate at a series of predefined locations. Local voltammetric experiments are carried out to construct an EC activity map. Due to the relatively smaller size of a single channel nanopipette, direct topographical/EC imaging is achieved with much higher spatial resolution.

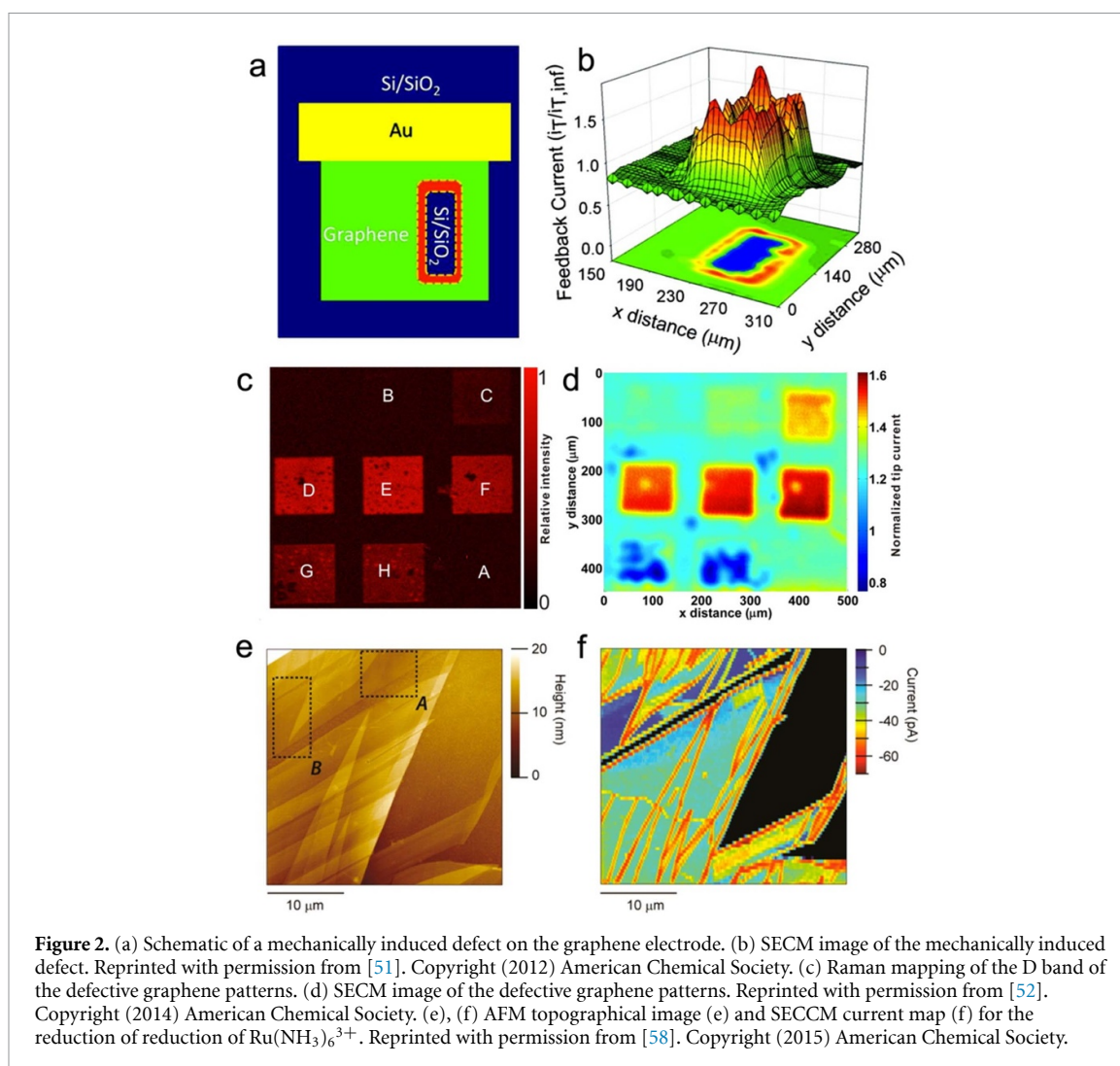
In comparison with SECM, SECCM is advantageous for being easier to implement. The pipette probes used in SECCM are easily fabricated at sizes smaller than typical microelectrodes. Since the electroactive area is dictated by the meniscus contact, the spatial resolution is determined by the nanopipette size and surface wetting, and is free from interference of diffusional broadening [21]. The modes of operation are straightforward, as EC current associated with either outer-sphere or inner-sphere reactions is directly measured.

3. Graphene and its derivatives

The isolation of graphene from graphite by mechanical exfoliation from graphite and the discovery of its exotic electronic properties [45, 46] ignited fundamental and applied research on graphene. Graphene and its derivatives have been of significant interest as electrode materials due to their high conductivity and tunable chemical/physical properties [8, 47]. The EC performance of these materials can be controlled by a range of methods that include stacking type, structural defects, chemical doping, and surface modification. Understanding how these fundamental factors influence interfacial activity is critical for exploring new directions in sensing and energy conversion/storage. In this section, we provide an overview of prior work on graphene and its derivatives, and discuss the unique benefits offered by spatially resolved EC information in elucidating the structure–function relationship of graphene-based electrodes.

3.1. Heterogeneous electron transfer (HET)

The kinetics of HET reactions are strongly influenced by the electronic structure, the energy level

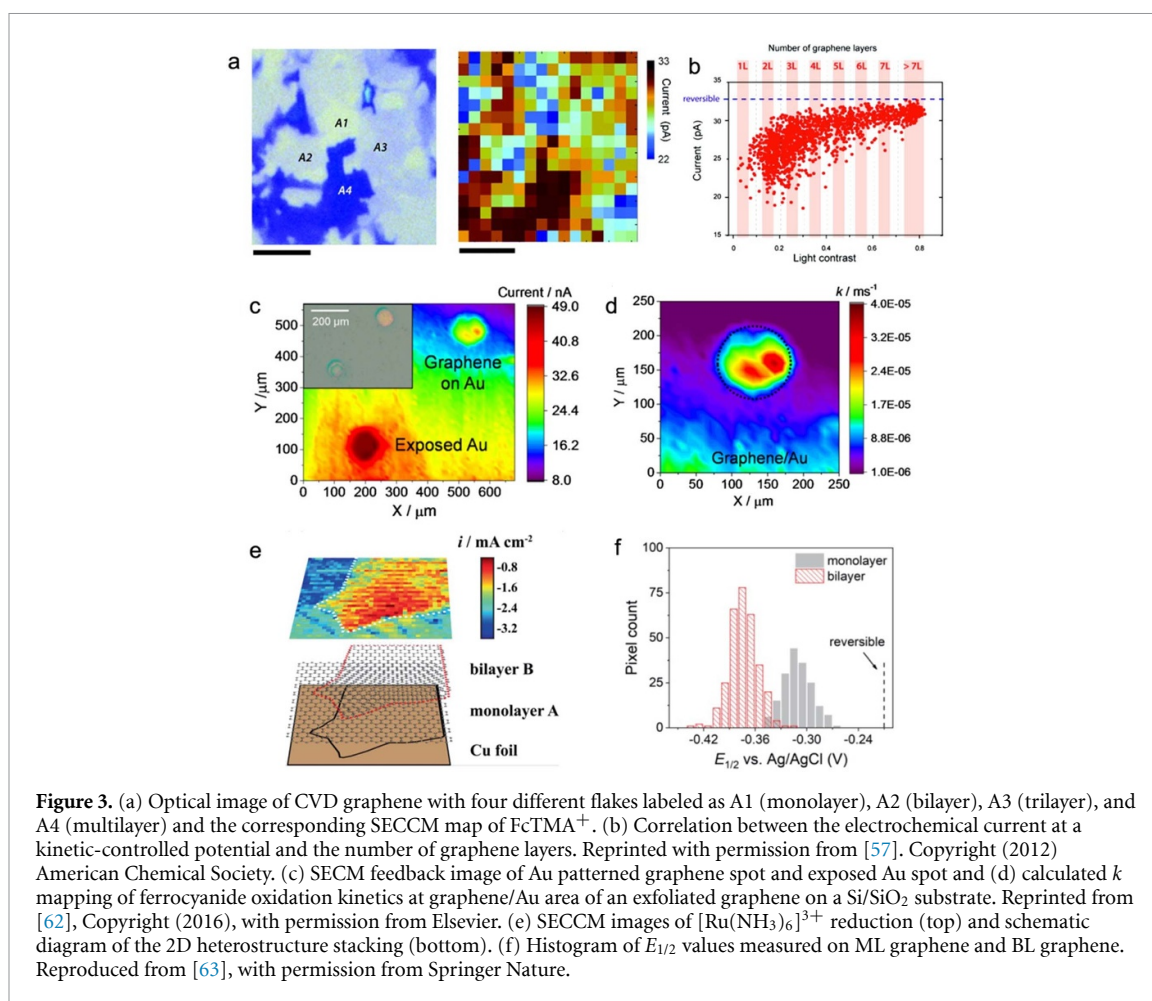


of the redox molecule, and electrolyte properties [48]. Pristine (undoped) graphene is a zero-bandgap Dirac semimetal with its conduction and valence bands meeting at the charge-neutrality/Dirac point and a vanishing electronic density of states (DOS) at the Fermi level. The basal plane of graphene has been reported to allow rapid HET of a variety of redox mediators both in aqueous and organic media [49, 50], and structural defects such as vacancies, adatoms, and grain boundaries have also been shown to strongly influence the electronic characteristics of graphene and thus impacts its HET behavior.

3.1.1. Defects and edges

SECM has demonstrated its powerful capability to interrogate the roles of defects at electrode surfaces. Tan *et al* examined the HET kinetics at the defect of CVD graphene and its surrounding areas were using SECM feedback imaging [51] as shown in figures 2(a) and (b). Much higher feedback currents were observed at the defect edges than over the surfaces far from the defects indicating more facile electron transfer kinetics at the defective sites.

The higher activities were attributed to the exposed edges and the chemical oxidation of sp^2 carbon centers in an aqueous environment. A more quantitative SECM study of the defect effects on HET kinetics was reported by Zhong *et al* [52]. Raman spectroscopy was used to determine the defect density from the intensity of the D peak activated by structural defects (figure 2(c)). The SECM feedback current images (figure 2(d)) are well correlated with the Raman D-band mapping in indicating that HET kinetics (characterized by the heterogeneous ET rate constant, k^0) have a strong dependence on the defect density. The enhanced HET kinetics at relatively low defect density regions ($<10^{13} \text{ cm}^{-2} \text{ s}^{-1}$) was explained as resulting from the formation localized electronic states associated with the point defects producing high local DOS that increases the overlap between the electronic states of graphene and redox molecules. The correlation between Raman spectra and SECM was developed further by the work of Schorr *et al* in which the EC effects of graphene oxidation were assessed in real time [53]. By correlating the Raman signatures of the graphene surface to the SECM



response, the effects of exfoliation, defect density, and surface modification/passivation on EC response were isolated.

A comparison of HET kinetics at graphene edge sites and basal planes has been extensively investigated for both natural graphite and highly oriented pyrolytic graphite (HOPG) [54–56]. The transition from bulk scale to mono/few-layer graphene has been largely explored by SECCM and microdroplet techniques [57–60]. To probe the behaviors of graphene edges, Güell *et al* applied SECCM to image exfoliated graphene on SiO_2 -coated Si wafers using $\text{Ru}(\text{NH}_3)_6^{3+/2+}$ couple whose redox potential lies close to the intrinsic Fermi level of graphene [58]. The AFM image and correlated SECCM map of the exfoliated graphene (figures 2(e) and (f)) evidently show that the regions with the highest HET activities are step edges. This dependence was attributed to the overlap in the DOS of the edge (defect) and basal graphene with the states of the $\text{Ru}(\text{NH}_3)_6^{3+/2+}$ redox couple.

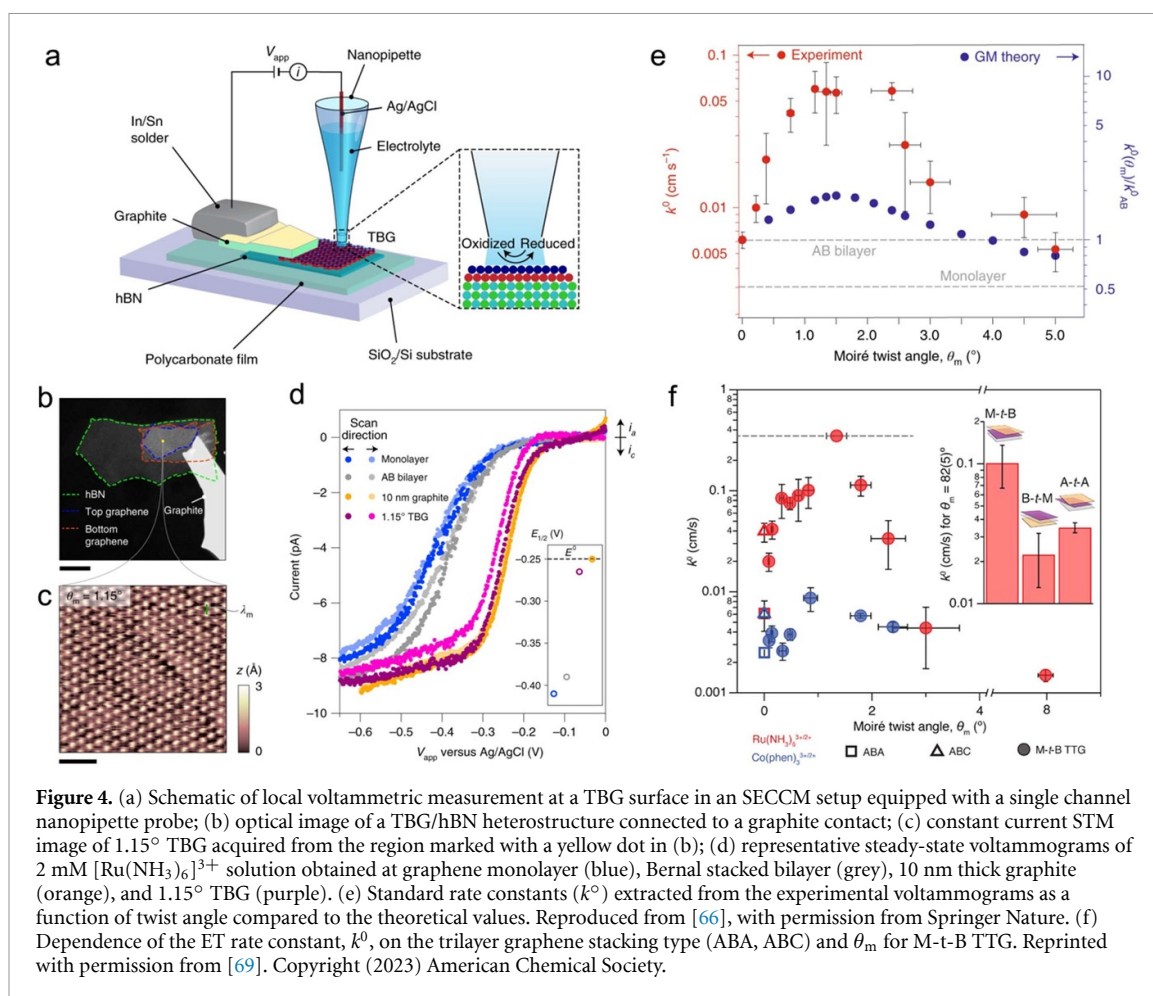
3.1.2. Thickness

The thickness dependence of graphene HET was studied by Güell *et al* with SECCM [57]. Dual channel pipettes filled with FcTMA^+ solution served as probes to obtain local voltammograms

at the graphene surface. Comparison between the topography revealed by optical microscopy and the SECCM current map (figure 3(a)) showed a clear correlation between the HET activity and the number of graphene layers. The local EC current as a function of the layer number (figure 3(b)) clearly shows a systematic increase of the HET kinetics with the number of layers until the point where HET becomes reversible, consistent with the evolution of increasing electronic DOS through single layer, bilayer, and multilayer graphene.

3.1.3. Substrates

The substrate under graphene layers plays an important role in modulating the HET kinetics owing to the effects of carrier doping and electrostatic interactions [61]. Hui *et al* reported on the modulation of the HET kinetics of outer-sphere redox mediators by metal electrodes buried in the sub-surface of continuous double layer graphene electrodes [62]. Figures 3(c) and (d) shows an increase in feedback current and rate constant (k) of $\text{Fe}(\text{CN})_6^{3-/4-}$ at the graphene-covered Au area compared with bare graphene, although this enhancement is smaller than exposed Au. Liu *et al* examined the EC kinetics at Cu-supported graphene layers using SECCM and co-located structural microscopy [63]. The SECCM



map (figure 3(e)) and $E_{1/2}$ histogram (figure 3(f)) of $\text{Ru}(\text{NH}_3)_6^{3+/2+}$ couple reveals that the HET kinetics follow the trend monolayer > bilayer > multilayer graphene. Varying the number of graphene layers modifies the electrostatic potential felt by the redox couple, which, in turn, changes the activation barrier for the reaction. In addition to these imaging-based studies, Chen *et al* investigated the effect of the poly(methyl methacrylate) (PMMA) supports on the HET behavior of $\text{FcMeOH}^{0/+}$ couple at CVD-grown graphene with SECM nanogap voltammetry [64]. The electrostatic charges of the underlying PMMA film were shown to impact the access of charged redox molecules to graphene, yielding varying transfer coefficients (α) and standard rate constant.

3.1.4. Twistrionics

The idea of twisting stacked 2D layers to manipulate their electronic properties gained rapid popularity in 2018 when it was discovered that bilayer graphene with a twist angle of $\sim 1.1^\circ$ (the so-called magic angle) behaves as a superconductor [65]. Recently, the concept of 'twistrionics' has been extended to control the HET at graphene materials by the interlayer twist angle. Yu *et al* employed SECCM (figure 4(a)) to selectively probe the EC kinetics of $\text{Ru}(\text{NH}_3)_6^{3+/2+}$ at the basal planes of twisted bilayer graphene (TBG)

[66] stacked on boron nitride layers (figure 4(b)). Scanning tunneling microscopy (STM) and SECCM (figures 4(c) and (d)) were used to visualize the moiré patterns [67] formed by twisting layers and obtain local steady-state voltammograms, respectively. The intriguing angle dependence of the HET kinetics (figure 4(e)) was attributed to spatial variation in the TBG reactivity due to localization effects of the flat band and the associated lattice reconstruction [67, 68] at angles $< 1.5^\circ$. Zhang *et al* extended the study to twisted trilayer graphene (TTG) and discovered that HET rates are strikingly dependent on electronic localization in each atomic layer [69]. Figure 4(f) shows the strong, nonmonotonic variation in k^0 of $\text{Ru}(\text{NH}_3)_6^{3+/2+}$ at TTG similar to the behavior of TBG. Importantly, a rotationally misaligned monolayer on a Bernal stacked bilayer (M-t-B structure) shows the greatest HET kinetics, suggesting the DOS enhancements are distinctly localized on the top two layers of M-t-B structures. In both studies, SECCM was leveraged to selectively probe twisted basal planes to exclude the effects from defective edges.

In summary, the simple reaction mechanisms of outer-sphere HET allow SECCM feedback imaging and SECCM mapping to be employed for effectively visualizing the spatial variations of HET kinetics at graphene electrodes. Coupled with other

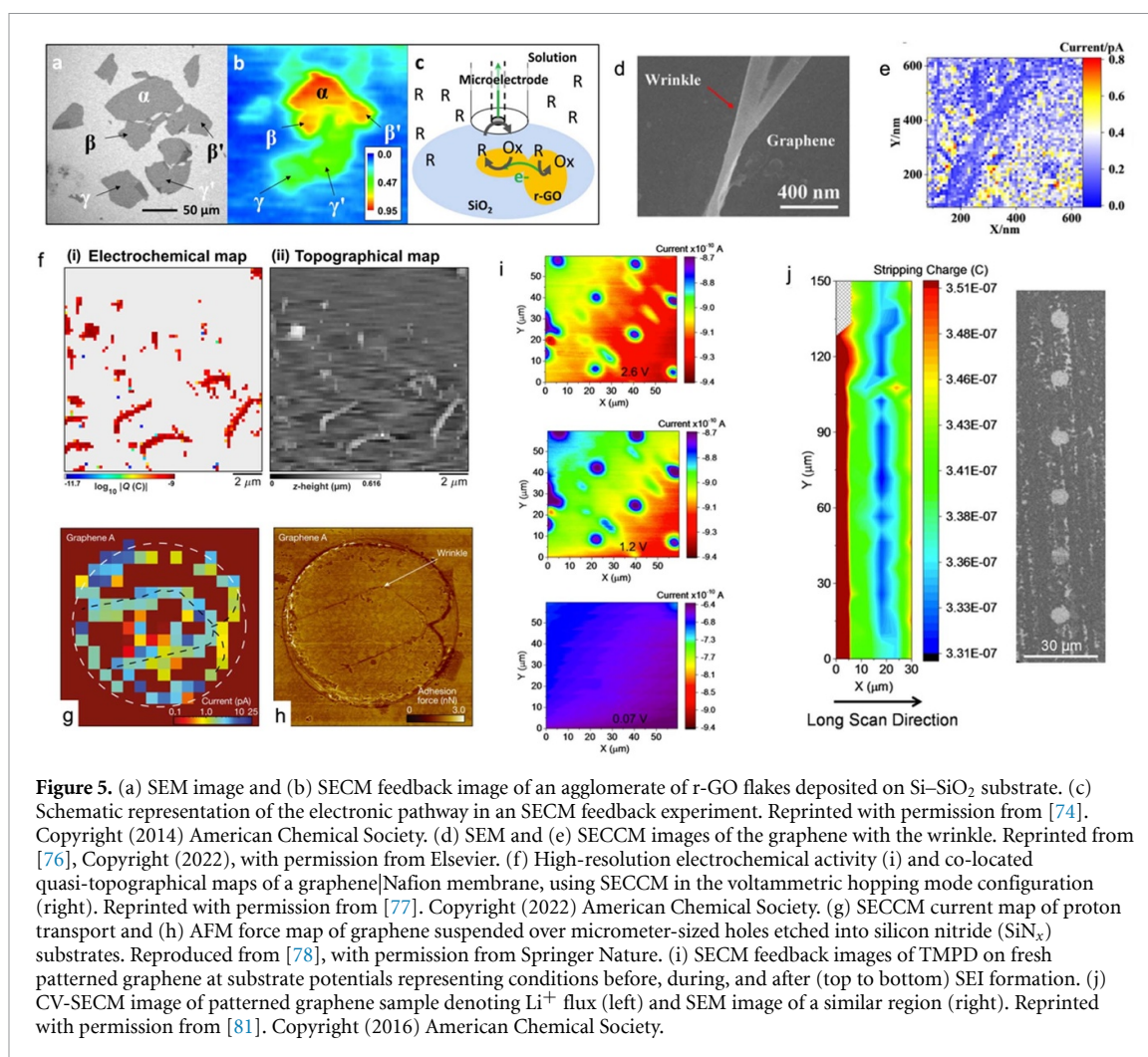


Figure 5. (a) SEM image and (b) SECCM feedback image of an agglomerate of r-GO flakes deposited on Si-SiO₂ substrate. (c) Schematic representation of the electronic pathway in an SECCM feedback experiment. Reprinted with permission from [74]. Copyright (2014) American Chemical Society. (d) SEM and (e) SECCM images of the graphene with the wrinkle. Reprinted from [76]. Copyright (2022), with permission from Elsevier. (f) High-resolution electrochemical activity (i) and co-located quasi-topographical maps of a graphene/Nafion membrane, using SECCM in the voltammetric hopping mode configuration (right). Reprinted with permission from [77]. Copyright (2022) American Chemical Society. (g) SECCM current map of proton transport and (h) AFM force map of graphene suspended over micrometer-sized holes etched into silicon nitride (SiN_x) substrates. Reproduced from [78], with permission from Springer Nature. (i) SECCM feedback images of TMPD on fresh patterned graphene at substrate potentials representing conditions before, during, and after (top to bottom) SEI formation. (j) CV-SECM image of patterned graphene sample denoting Li⁺ flux (left) and SEM image of a similar region (right). Reprinted with permission from [81]. Copyright (2016) American Chemical Society.

characterization techniques such as Raman spectroscopy and AFM [70], factors including defects, thickness, and substrate were better understood using correlative studies. In addition to these mapping experiments, nanogap voltammetry realized in SECM was shown to be effective in determining rapid kinetics, while local voltammetry in SECCM allowed researchers to obtain EC measurements exclusively at the basal plane of the constructed graphene heterostructures.

3.2. Electronic and ionic transport

The electronic properties of graphene and its derivatives result in distinctive inter- or intra-layer transport properties, which can manifest in EC measurements [1]. The reversible intercalation of mobile ions into the interlayer gaps of layered materials plays a key role in EC energy storage applications [71, 72]. SECM and SECCM have been employed to acquire spatially resolved EC data that shed light on the transport of charge and ions.

3.2.1. In-plane electron transport

The effects of in-plane electron transport on graphene electrochemistry have been mainly investigated using SECM feedback mode. Azevedo *et al* used

SECM to obtain surface conductivity maps of heterogeneous graphene oxide (GO) thin films deposited on glass [73]. The conductivity was approximated as a function of the feedback current, providing a general and simplified framework for quantitative conductivity mapping. Bourgeteau *et al* used SECM to investigate the electronic conduction of individual and interconnected reduced graphene oxide (r-GO) flakes [74], using SECM feedback measurements to map the EC activities of interconnected and isolated r-GO flakes deposited on Si/SiO₂ substrates (figure 5(b)). The redox cycling reaction at the substrate and positive feedback is necessarily associated with a counter reaction occurring elsewhere as depicted in figure 5(c). This indicates that the inter-flake contact resistance impacts the transport of electrons in r-GO-based materials. A similar SECM approach was used to characterize the role of contact resistance in the electrochemistry of MoS₂ flakes [75]. A solid-state SECCM was created using polyacrylamide as a solid electrolyte to probe the electrochemistry of wrinkled graphene [76]. Correlated SEM (figure 5(d)) and SECCM (figure 5(e)) images revealed lower current at the two sidewalls of the wrinkles compared to center of the wrinkle and

the planar surface of graphene, suggesting a slower electron transfer rate at the wrinkle. This is because electrons need to climb over the nanoscale wrinkle, which restricts electron transport and leads to a low EC activity. This high spatial SECCM study provided the first and direct evidence of the electron transfer mechanism at the wrinkles.

3.2.2. Interlayer ion permeability

Graphene has been increasingly explored as an ion-selective membrane for diverse applications. Bentley *et al* captured ion-flux images at a graphene|Nafion membrane using an SECCM [77]. The SECCM configuration represented as an EC ion (proton) pump cell was employed to detect local proton transport across the graphene film in one direction in response to the proton-consuming reactions at the underlying Pt electrode. SECCM scanning of ion transport (figure 5(f)) revealed that the majority of the CVD graphene overlayer does not conduct protons, while proton transmission was noted to be highly localized in areas of the graphene film that contained atomic defects. Wahab *et al* later demonstrated that proton permeation through defect-free graphene and hexagonal boron nitride is greatly facilitated by nanoscale non-flatness where strain is accumulated [78]. Figures 5(g) and (h) show clear wrinkles and edges in the AFM maps that correlate well with high-conductivity areas in the SECCM maps. The nanoscale ripples that are ubiquitous in 2D membranes result in considerable strain, accelerating proton transport due to lowered energy barrier for proton permeation. The discovery that strain and curvature can amplify proton conductivity in 2D crystals holds promise for diverse applications. This work further reinforces SECCM as an effective tool for resolving ion transport through 2D materials.

3.2.3. Ion insertion

Significant research interest related to energy storage has focused on exploring the intercalation dynamics and the evolution of electrode structures [79, 80]. Importantly, SECM has been shown to be a potentially powerful tool to characterize the surface conductivity and ion flux distribution during ion intercalation at graphite and few layers of graphene.

Hui *et al* used SECM to demonstrate changes in the surface conductivity throughout the evolution of the solid–electrolyte interphase (SEI) upon Li^+ intercalation in a few-layer graphene [81]. SECM operated in feedback mode was used to image the spatially resolved HET activity of TMPD redox reaction at a patterned multilayer graphene electrode at various stages of SEI formation (figure 5(i)). The substrate potential at 2.6, 1.2, and 0.07 V vs Li/Li^+ denotes the condition before, during, and after SEI formation, respectively. The SECM image at 2.6 V shows good contrast between patterned holes and the graphene

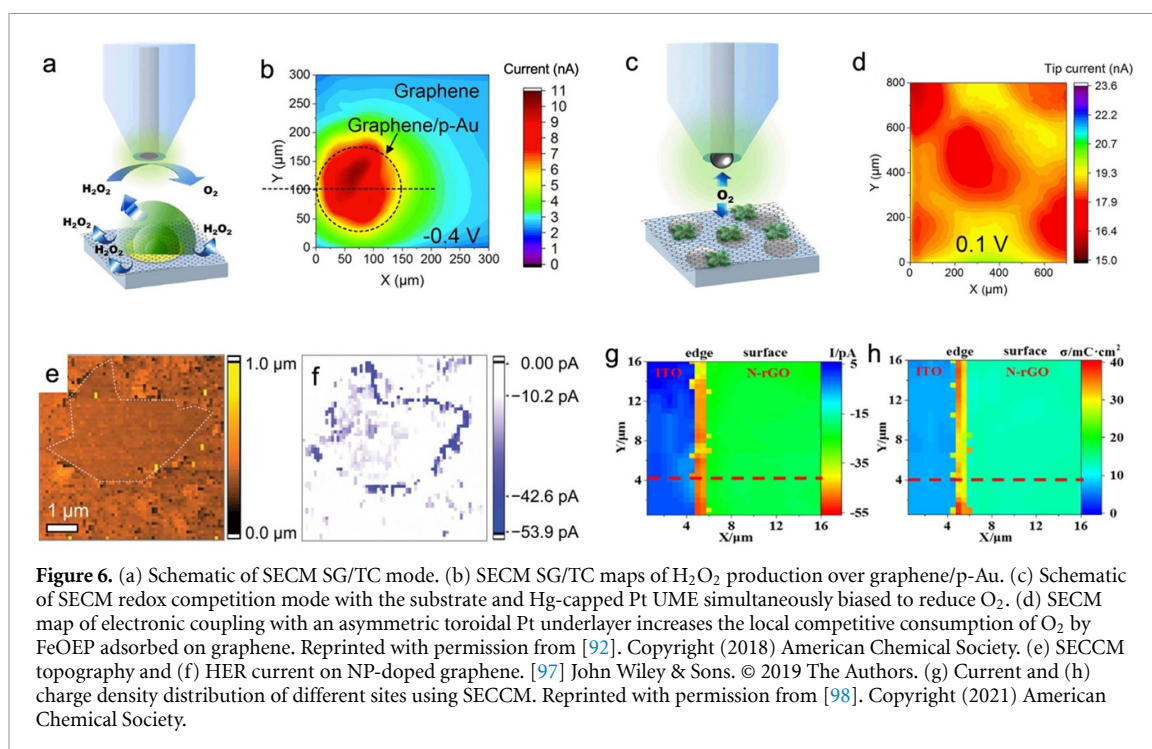
surface, demonstrating fast electron transfer kinetics at pristine graphene. As the potential is ramped negatively to induce SEI formation, a reduction in tip feedback response is noted, attributed to diminished substrate kinetics. At 0.07 V, the pattern became indistinguishable, providing solely negative feedback to the tip signal. This series of SECM images clearly reveal that stable and condensed SEI layer blocks electron transfer. The spatial variation of Li^+ conductivity was investigated by employing an Hg-capped ultramicroelectrode [82] as a selective Li-ion sensor to quantify Li^+ uptake into multilayer graphene with a formed SEI layer. The blue spots in the SECM image (figure 5(j)) represent areas of lower Li^+ concentration (therefore a larger inward Li^+ flux), matching well with the spatial distribution of the etched openings. These observations demonstrate that Li ions migrate into graphene interlayers more efficiently through the edge planes. This work was the first time that SECM is used to visualize ionic fluxes through an SEI on a battery material in real time.

Similar SECM approaches were developed to map Li^+ flux and electron transfer reactivity during SEI formation at a graphene electrode [83, 84]. The correlated maps revealed that location-specific uptake of Li^+ was closely associated with heterogeneous substrate distribution in feedback mapping. By developing a model of the intercalation process, the authors determined localized kinetic information of reversible Li^+ (de)intercalation on edge planes. SECM also allowed *in-situ* interfacial analysis of incipient SEIs in various alkali-ion electrolytes formed on multilayer graphene [85]. By correlating SECCM measurements with XPS results, the authors observed substantial formation of metal fluorides in the Li^+ and Na^+ electrolytes, whereas there was no appreciable formation in the K^+ electrolyte. Sarbapalli *et al* further presented SECM experimental evidence of Na^+ intercalation in fluorinated few-layer graphene [86]. It was discovered that reversible Na^+ intercalation necessitates a pre-existing Li-based SEI alongside surface fluorination.

In summary, these studies have underscored the promise of SECM/SECCM as tools for characterizing nanoscale electronic and ion flux at graphene and related materials. Importantly, the dynamics of in-plane electron transport, ion transport across layers, and surface conductivity modulation were translated to the HET responses that were readily analyzed by SECM/SECCM.

3.3. Electrocatalysis

A fundamental challenge in developing metal-free electrocatalysts (e.g. graphene-based materials) for sustainable energy conversion chemistry lies in the low intrinsic catalytic activity of graphene [87]. General strategies to improve the reactivity of pristine graphene basal planes include heterostructure construction [88] and heteroatom doping [89],



since these routes can be used to tune electronic states and optimize the adsorption energies of key intermediates. Scanning EC probe techniques have been employed to mechanistically investigate the catalytic performance of graphene-based electrocatalysts optimized by these strategies.

3.3.1. Substrates

Electroactive materials adjacent to graphene layers have a strong impact on the electrocatalytic activity of graphene. The carrier doping effects induced by underlying metallic materials are well known to modulate the electronic structure and DOS of the top graphene layer [90, 91].

Hui *et al* demonstrated the SECM study on the electronic effects induced by an underlying Au substrate on the graphene reactivity toward oxygen reduction reaction (ORR) [92]. The H_2O_2 generation from a two-electron reduction of O_2 at CVD-grown graphene was spatially investigated via an SECM SG/TC mode (figure 6(a)). Higher collection current of H_2O_2 over the graphene/p-Au spot (figure 6(b)) reveals ORR kinetics enhanced by underlying metal. This aligns with their calculated electronic structure, where the electronic DOS of the heterostructures is dominated by the metal, particularly the d-subshell of Au. These findings underscore the significant catalytic benefits attained through the incorporation of underlayer metal supports for graphene. SECM competition mode was then used to explore the charge coupling effects between metal underlayers and adsorbed molecular catalysts (FeOEP) on graphene (figure 6(c)). Higher consumption rate of O_2 by the substrate is reflected by decreased tip current. The agreement between the current distribution

and the known metal underlayer geometry supports the conclusion that enhanced ORR is attributable specifically to electronic donation from the Pt underlayer to the molecular overlayer through the electronically ‘semi-transparent’ graphene interface (figure 6(d)).

Schorr *et al* investigated the effects of plasmonic Au nanoparticles as an underlying substrate on the ORR reactivity of graphene with SECM [93]. The ORR kinetics obtained from H_2O_2 collection by SECM tip followed the temperature dependent Arrhenius behavior, suggesting that the photo-thermal effects other than hot carriers are primarily responsible for the enhanced EC reactivity. Substrate effects on the electrocatalytic hydrogen evolution reaction (HER) activity of a hexagonal boron nitride [94] (hBN, also known as ‘white graphene’) layer was studied using the SECCM technique [95]. Local voltammetry and Tafel analysis reveal that Au-supported hBN exhibiting significantly enhanced HER kinetics compared to h-BN/Cu. The authors postulated that this is due to the modulation of hydrogen adsorption energy caused by the electronic interaction of hBN with the underlying metal substrate.

3.3.2. Doping

Heteroatom doping is an effective approach to tailor the electronic properties of graphene for efficient surface chemistry. Introducing high electronegativity atoms such as N, B, and P in the graphene lattice forms new active sites [89]. Multi-doped materials show even higher electrocatalytic activities [96]. New Insights into the doping effects were gained through the following SECCM studies.

Kumatani *et al* investigated the synergetic effects of the edge structure and N/P doping on the

HER activity of a graphene-based electrocatalyst with SECCM [97]. They synthesized edge-enriched graphene with N and P dopants that predominantly reside near the graphene edges. Figures 6(e) and (f) show the SECCM topology and on-site HER current map for the NP-doped graphene samples. Comparison between the topology data and the current mapping reveal that the edge region is more active in HER. Specifically, the turnover frequency values for chemically doped graphene were observed to be approximately 100–200 times greater at the edges compared to the planar regions. The presence of edges introduces geometric frustration to the graphene lattice, facilitating the accumulation of chemical dopants, whereas defect-free regions promote electron transfer to the edge sites. Consequently, these regions synergistically contribute to the enhancement of reaction kinetics. This study directly demonstrates that the combination of chemical doping and edge engineering drastically boosts the HER activity.

SECCM was used to investigate the origins of enhanced EC activity at edges of N-doped reduced graphene oxide (N-rGO) [98, 99]. Local EC impedance spectroscopy coupled with SECCM revealed larger double-layer capacitance and smaller interfacial resistance in the edges [99]. Jin *et al* extended the SECCM study to the HER reaction at N-rGO microsheets [98]. Non-faradic and faradic currents from the total currents were isolated to map the charge accumulation and EC activity, respectively. The HER current map (figure 6(g)) and charge density map (figure 6(h)) provided a direct correlation between the activity and the accumulated charge at the active sites, showing that charge accumulation at edges has a great effect on promoting the catalytic performance. This direct evidence will be significant for a deep understanding of the mechanism of the HER process at highly catalytic materials.

Dechant *et al* applied SECCM to investigate the link between the geometry and EC activity of nitrogen and sulfur (NS) doped 3D curved graphene [100]. The elemental mappings demonstrated the distribution of NS dopant atoms at the curved regions rather than the flat regions. SECCM mapping of the on-site HER current clearly demonstrates the dependence of activity on morphology, i.e. higher current was observed at highly curved topographies. The curved graphene induced topological defects and enhanced the electronic DOS, resulting in Gibbs free energy of hydrogen adsorption be nearly zero owing to the cooperation of the dopants near the topological defect sites.

Indeed, heteroatom doping introduces supplementary parameters for fine-tuning catalytic activity. Spatially resolved measurements with SECCM are deemed indispensable for elucidating the synergistic interplay between dopants and structural heterogeneities.

3.4. Surface functionalization

Modified graphene is often used for enhancing the specific absorption of analytes and anchoring molecules/nanoparticles. While this topic has been extensively reviewed [101, 102], this section focuses on the applications of SECM in local EC functionalization of graphene surface and characterization of functionalized molecules.

SECM as lithographic tools are useful for local surface EC modifications at different scales by tuning the probe size and scanning range [103–105]. Generally operated in TG/SC mode (or direct mode), the reactions controlled by the tip electrode induced local chemical events that modify the underlying substrate. Azevedo *et al* introduced an SECM approach for local functionalization of thin GO films [36]. The *in-situ* generation of naphthalene radical anions by an SECM tip electrode placed in the vicinity of the GO substrate resulted in a localized reduction of GO associated with the formation of conductive r-GO patterns. Smaller tip size and higher displacement speed lead to higher spatial resolution and more confined reduction spot. The local transformation of GO into r-GO permitted a selective electro-grafting of diazonium layer which was used to immobilize Au nanoparticles. Torbensen *et al* modified the graphene surface with carboxylate groups via CO₂ reduction by SECM [106]. The process was carried out with spatial control together with the degree of carboxylation manipulated by the EC potential and reaction time.

SECM has been employed to characterize the functionalized molecules and their effects on the EC behavior. Pham-Truong *et al* modified graphene with p-nitrophenyl diazonium and used SECM to probe the changes introduced in the HET kinetics [107]. The kinetic parameters obtained from approach curves demonstrate that the attached nitrophenyl layer accelerates the HET kinetics. Rodríguez-López *et al* used SECM to investigate the activity of a tripodal molecular motif adsorbed on a monolayer graphene and quantify its surface diffusion [108]. Using the SG/TC mode of SECM, they concluded that the catalytic tripod produced H₂O₂ more rapidly than the bare graphene surface in the ORR. The evolution of the SECM images suggested that the activity at the tripodal spots decreased over time. This behavior was attributed to decreased surface concentration of the molecular catalyst due to diffusion, demonstrating how the SECM technique is an important approach for understanding the effects of mass transport in graphene functionalization as well as molecular electrocatalysis.

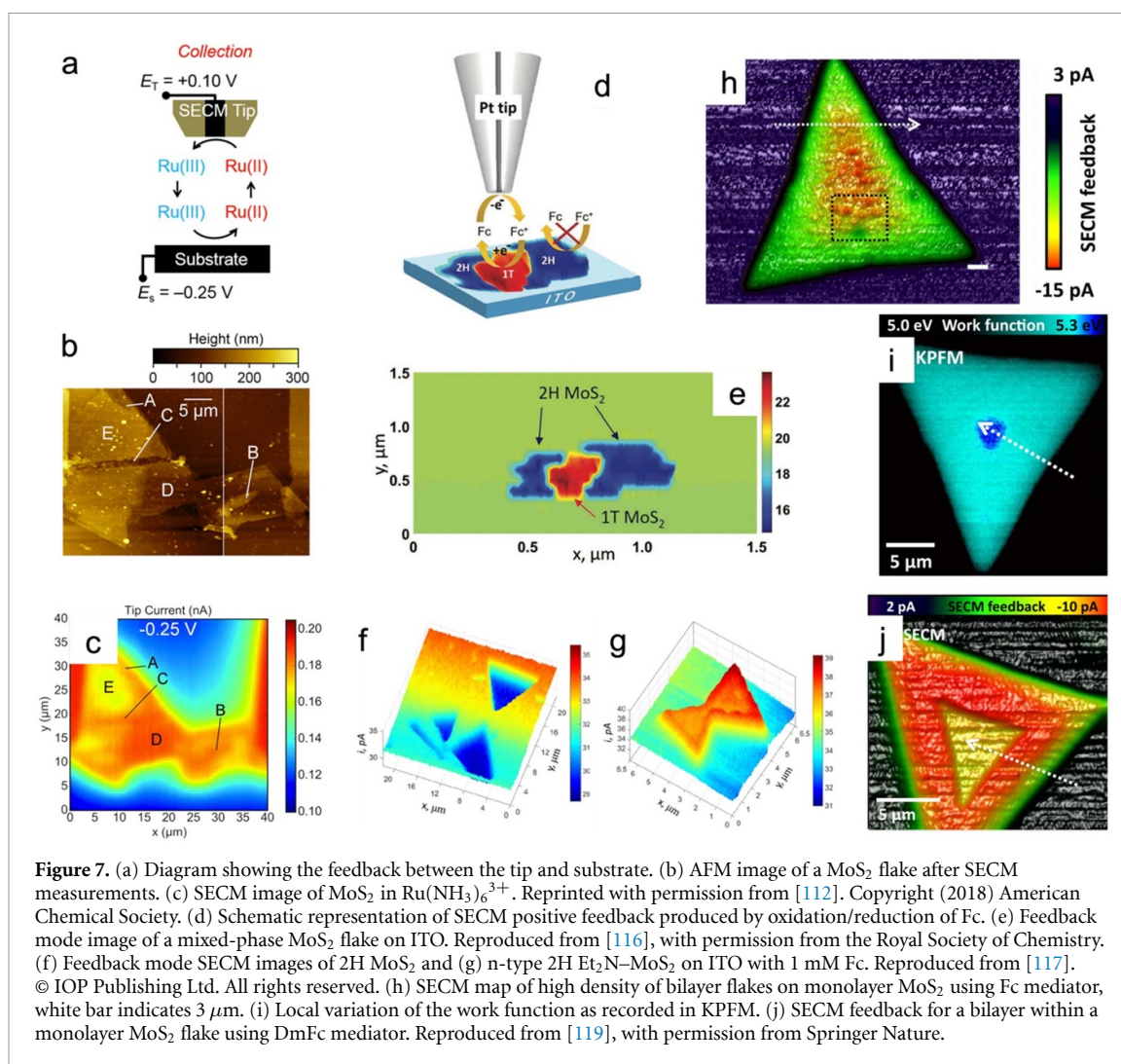
In table 1 we summarize SECM/SECCM work on graphene and its derivatives. A wide of range of outer-sphere redox reactions and catalytic reactions demonstrate the versatility of graphene electrode. In addition to elucidating intrinsic factors influencing HET

Table 1. Summary of scanning electrochemical studies of graphene and its derivatives.

Technique/mode	Materials	Reactions	References
SECM feedback	CVD graphene	FeEDTA ^{3-/4-} , Ru(CN) ₆ ^{3-/4-} , Fe(CN) ₆ ^{3-/4-} , CoSep ^{3+/2+} , FcMeOH ⁺⁰ , Mo(CN) ₈ ^{3-/4-} , MV ⁺⁰ , Ru(NH ₃) ₆ ^{3+/2+} , Ru(bpy) ₃ ^{3+/2+} , Fc ⁺⁰ , Co(dapa) ₂ ^{3+/2+}	[50]
SECM feedback	CVD graphene	FcMeOH ⁺⁰ , Fe(CN) ₆ ^{3-/4-}	[51]
SECM feedback	Defective CVD single layer graphene	FcMeOH ⁺⁰	[52]
Raman-SECM feedback	CVD multilayer graphene	FcMeOH ⁺⁰ , Fe(CN) ₆ ^{3-/4-}	[53]
SECCM, double-barreled pipette	CVD graphene	FcTMA ^{2+/+}	[57]
SECCM, double-barreled pipette	Mechanically exfoliated graphene	Ru(NH ₃) ₆ ^{3+/2+}	[58]
SECM feedback	CVD graphene on Au	Fe(CN) ₆ ^{3-/4-} , Fc ⁺⁰	[62]
SECCM hopping mode	CVD graphene on Cu	Ru(NH ₃) ₆ ^{3+/2+}	[63]
SECM feedback	GO, r-GO	FcMeOH ⁺⁰ , Ru(NH ₃) ₆ ^{3+/2+} , [Fe(CN) ₆] ^{3-/4-}	[61]
SECM feedback	CVD graphene	FcMeOH ⁺⁰	[64]
SECCM, single-channel pipette	Twisted bilayer graphene/h-BN	Ru(NH ₃) ₆ ^{3+/2+} , Co(Phen) ₃ ^{3+/2+}	[66]
SECCM, single-channel pipette	Twisted trilayer graphene/h-BN	Ru(NH ₃) ₆ ^{3+/2+} , Co(Phen) ₃ ^{3+/2+}	[69]
SECM feedback	r-GO	FcMeOH ⁺⁰	[73]
SECM feedback	r-GO	Fc ⁺⁰	[74]
All-solid SECCM	Multilayer CVD graphene	Fe(CN) ₆ ^{3-/4-}	[76]
SECCM, double-barreled pipette	Monolayer CVD graphene	H ⁺ permeation	[77]
SECCM, double-barreled pipette	Mechanically exfoliated graphene and h-BN	H ⁺ permeation	[78]
SECM feedback, ion-sensitive SECM	Multilayer CVD graphene	TMPD ⁺⁰ , Li ⁺ (de)intercalation	[81]
SECM feedback, ion-sensitive SECM	CVD graphene	Li ⁺ intercalation, TMPD ⁺⁰	[83]
SECM feedback, ion-sensitive SECM	Multilayer CVD graphene	Li ⁺ , Na ⁺ , K ⁺ intercalation, Fc ⁺⁰	[85]
Ion-sensitive SECM	Fluorinated few-layer CVD graphene	Na ⁺ intercalation	[86]
SECM SG/TC	CVD graphene on metal substrates	ORR	[92]
SECM feedback and SG/TC	CVD graphene on AuNP arrays	FcMeOH ⁺⁰ , ORR	[93]
SECCM hopping mode	h-BN on metal substrates	HER	[95]
SECCM, single-channel pipette	Edge-enriched N-doped, P-doped, NP-codoped CVD graphene	HER	[97]
SECCM, single-channel pipette	N-doped r-GO	HER	[98]
SECCM-LEIS	N-doped r-GO	Fe(CN) ₆ ^{3-/4-}	[99]
SECCM hopping mode	CVD curved graphene, NS-doped graphene	HER	[100]
SECM, direct mode	GO	GO reduction, dopamine	[103]
SECM, direct mode	GO	reduction of naphthalene, GO reduction	[36]
SECM, direct mode	Multilayer CVD graphene	CO ₂ reduction, carboxylation of graphene	[106]
SECM feedback	Diazonium modified single layer CVD graphene on plastic film	TCNQ ^{0/-} , Fc ⁺⁰	[107]
SECM SG/TC and feedback	Tripodal compound adsorbed on single layer CVD graphene	ORR, Fe(CN) ₆ ^{3-/4-}	[108]

kinetics, SECM feedback experiments are proved powerful in addressing electronic and ionic transport. SECM GC mode was employed to detect intermediates in complex catalytic reactions and

perform local modification with high precision. SECCM served as a powerful tool to directly map surface activity variation in both HET and catalytic reactions.



4. Transition metal dichalcogenides (TMDs)

Two-dimensional transition metal chalcogenides (TMDs) are a class of van der Waals materials with structural and electronic properties that hold promise for a variety of applications in energy conversion and storage [109]. As electrocatalysts, some TMDs have been touted as candidates for low-cost and high-efficiency energy conversion [8, 110]. Layered TMDs can be described with the general chemical formula MCh_2 , where M is a transition metal element, and Ch is a chalcogen. The structural polytypes (phases), step edges, and other effects such as strain and the presence of atomic vacancies are considered key factors in determining the overall activity. In particular, the semiconducting 2H phases of group VI TMDs ($M = \text{Mo}, \text{W}$) with a direct bandgap in the monolayer limit can absorb light to generate photoexcited charge carriers for photoelectrochemical reactions. In this section, we summarize recent progress in investigating the rich (photo)electrochemistry of TMDs using scanning EC probe techniques.

4.1. Heterogeneous electron transfer (HET)

4.1.1. Defects

Like sp^2 carbon materials, HET reactions on MoS₂ proceed more readily at edge sites than at basal planes due to higher electron density [111]. Ritzert *et al* have demonstrated the spatial inhomogeneity in HET behavior of MoS₂ with submicron-resolution SECM [112]. The current at the SECM tip associated with the collection of electrogenerated Ru(NH₃)₆²⁺ was measured as a function of lateral tip position (figure 7(a)). Figures 7(b) and (c) show lowest reactivity on basal plane areas (region E), whereas regions possessing a trench (region C) and macrosteps (region A) consisting of a high density of edge sites were more active. Cabré *et al* further used the hopping mode of SECCM to map the EC reduction of Ru(NH₃)₆³⁺ on a 2D MoS₂ sample immobilized on Au substrate to detect nanoscale defects [113]. These defects give rise to EC responses that are equivalent to disk-shaped defects with radii of tens of nanometers in size, or to one-dimensional defects with nanometer to sub-nanometer widths. Importantly, only low densities of defects are

needed to dominate the EC response of the entire surface area.

4.1.2. Structural polytypes

The metallic $1T$ phase and the related $1T'$ phase of MoS_2 display dramatically distinct EC properties in comparison with the semiconducting $2H$ phase. Converting $2H$ to $1T$ or $1T'$ via phase engineering has been shown to be effective in enhancing the EC activities [114, 115]. Due to the metastable nature of the T phases, these polytypes transform back to the $2H$ phase over time. Simultaneous nanoscale resolution of morphology and activity via SECM is a viable approach to characterize the electrochemistry of a complex system containing mixed phases. Sun *et al* used SECM feedback mode (figure 7(d)) to spatially probe $1T$ and $2H$ domains within a mesoscopic MoS_2 crystal using ferrocenemethanol as the redox mediator [116]. A negative feedback response was obtained at $2H$ phase, while significant positive feedback was observed at the $1T$ phase. The activity map of the mixed-phase MoS_2 nanosheets shows that the $1T$ phase was sandwiched by the $2H$ phase with an abrupt boundary (figure 7(e)). This map suggested that the phase conversion appears to proceed from the outside of the flake inwards and along straight lines, which was likely caused by a sliding of the S atomic plane. Zhang *et al* demonstrated the stabilization of heavily n-type doped $2H$ and $1T$ MoS_2 monolayers with a low reversion to the initial phase [117]. The *n*-butyl lithium immersion treatment converts the $2H$ phase to n-type $2H/1T'$, while surface functionalization stabilizes the phase. SECM images showed higher tip currents over the surface-functionalized monolayer (figure 7(g)) than $2H$ MoS_2 (figure 7(f)), suggesting that the entire MoS_2 monolayer is homogeneously n-type doped and the converted $1T'$ phase was stable in the air.

4.1.3. Thickness

SECCM was leveraged to quantify the effect of the thickness of bottom-contacted 2D TMDs (MoS_2 , MoSe_2 , WS_2 , WSe_2) on the EC response of the $\text{Ru}(\text{NH}_3)_6^{3+/2+}$ redox couple [118]. The responses on all four materials were similar and showed a decrease in the electron transfer rate with an increase in layer thickness. This dependence was explained as resulting from by the electron transport process through the TMD layers—thicker layers resulting in less frequent electron tunneling and net slower transport from the bottom contact across the TMD layer to the TMD–electrolyte interface.

Another study by Du *et al* demonstrated that the HET behavior of unbiased MoS_2 flakes is affected by both layer numbers and redox mediator [119]. Ferrocene (Fc) and decamethylferrocene (DmFc) redox probes in organic solutions were used to elucidate the central relevance of the mediator on the band alignment and the localization effects in SECM

feedback experiments. A strong bilayer contrast was detected in SECM maps with a quantitative feedback enhancement of the order of 30% on top of the bilayer islands (figure 7(h)) when Fc was used as the redox mediator. Figure 7(j) demonstrates a reversed SECM feedback contrast when a more negative redox potential mediator (DmFc) was used for the otherwise identical sample system. The distinct behaviors were attributed to the work function differences (figure 7(i)) and how band offsets were aligned with unoccupied states of Fc^+ and DmFc^+ .

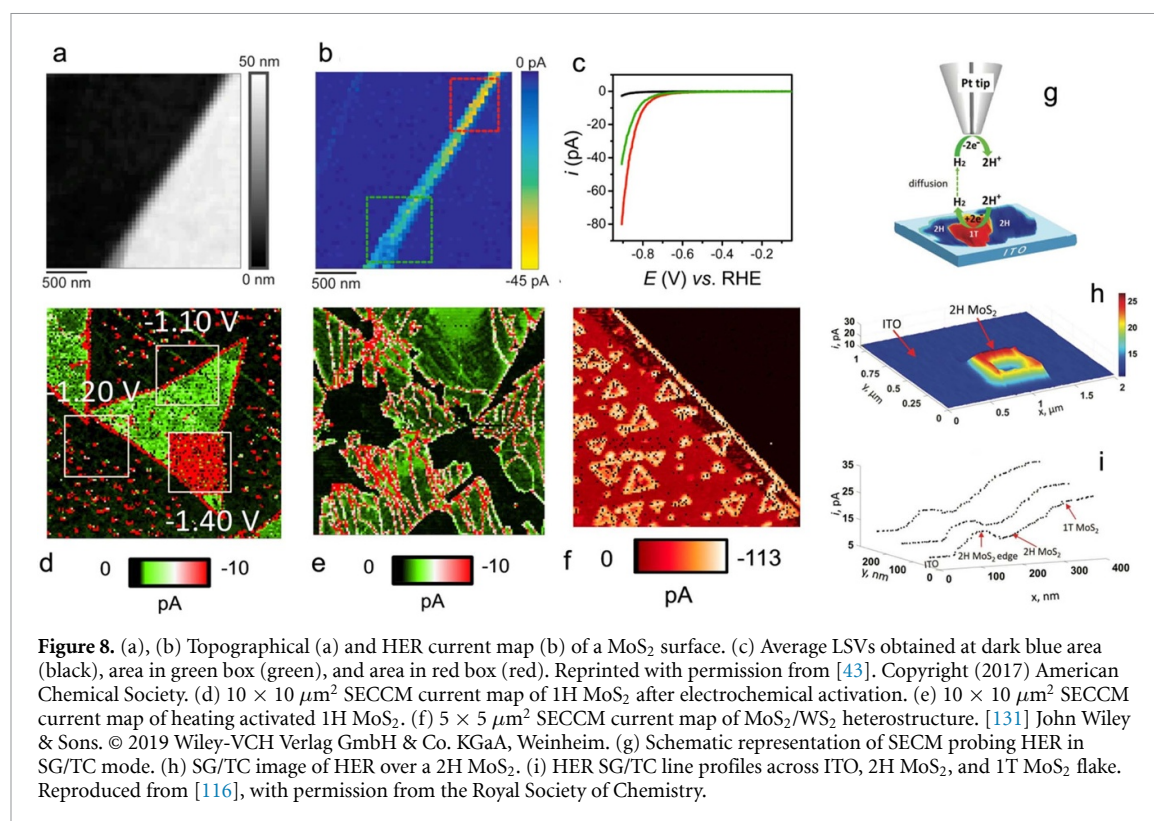
In contrast to graphene electrode, the HET at TMDs is predominately dictated by the carrier density and charge transport within the layer. The published work exploited the advantages of scanning probe electrochemistry to resolve the influence of defects, phase, thickness, and external electrostatic manipulation [120] to the charge carriers and the resultant HET activities.

4.2. Hydrogen evolution reaction (HER)

Two-dimensional (2D) TMDs have stimulated much interest in them from researchers in the field of HER electrocatalysis [121]. The overall reaction kinetics of the HER are largely dictated by the Gibbs free energy associated with hydrogen adsorption, ΔG_{H^*} . The adsorption energy is determined by the electronic structure of the catalyst surface [122], which can be tuned by doping, defect engineering, phase engineering, and strain engineering [123]. Spatially resolving HER activity across TMD layers with scanning EC probe techniques has been very useful for providing a mechanistic understanding of how these parameters impact electrocatalytic behavior.

4.2.1. Edges

The edges of MoS_2 have been proposed to be the active sites for HER from theory/computations [124] and experimental measurements [125]. The site-specific HER activities at MoS_2 surfaces have been extensively investigated by SECCM [126, 127]. For instance, Bentley *et al* carried out pixel-resolved linear-sweep voltammetry (LSV) at MoS_2 surfaces in acidic media using single channel nanopipettes to achieve a high spatial resolution [43]. The topographic map (figure 8(a)) and the HER current map (figure 8(b)) show relatively low yet uniform activity across the basal plane and enhanced HER kinetics at the edge planes. Local LSVs obtained on different spots shown in figure 8(c) distinctly manifest the variations in activity across the SECCM map. Important HER kinetic parameters such as exchange current densities and Tafel slopes, were evaluated separately on the basal planes and edge sites, a distinction that is unachievable with any bulk measurement approach. Tao *et al* expanded the SECCM study to WS_2 , showing similar activity variation between basal and edge planes [128]. The effects of surface aging were found to deteriorate catalytic activity, due to the build-up



of adsorbates and oxidation products, particularly at active edges.

4.2.2. Atomic vacancies

Introducing S vacancies to the MoS₂ lattice leads to the emergence of localized electronic states (associated with these S vacancies) within the bandgap. These S vacancy sites favor hydrogen adsorption on the TMD basal plane [129, 130]. Takahashi *et al* carried out SECCM measurements on the effects of defect engineering and TMD heterostructures [131]. The S vacancies on a 1H-MoS₂ monolayer were generated by EC desulfurization and controlled by the applied potential. The SECCM current map in figure 8(d) shows that the highest HER activity was observed in the area activated by a bias of −1.40 V vs. RHE, whereas no significant improvement was seen with less positive biases. The results suggest that a threshold voltage is required to generate S vacancies. The SECCM current map (figure 8(e)) shows superior activity of cracked regions similar to the edge planes. In addition, inhomogeneous HER activity was imaged at the surface of MoS₂/WS₂ heterostructures. In the SECCM current map shown in figure 8(f), the highest activity was observed at MoS₂ edges. The MoS₂ basal planes are slightly more active than WS₂ basal planes, but no distinctive catalytic activity was observed at the heterojunction. It has also been reported that the activation of the basal plane of MoS₂ by creating S vacancies can be further enhanced by an elastic strain that moves the midgap states closer to the Fermi level [132]. Li *et al* employed SECM SG/TC mode to determine the kinetic information on both

unstrained and strained S vacancies on the basal plane of MoS₂ monolayers [133]. The rate constant of the sample with 2% uniaxial tensile strain was found to be enhanced by almost four-fold, confirming that strain indeed accelerates the HER kinetics at MoS₂ with S vacancies.

4.2.3. Structural polytypes

The activation of the TMD basal planes via phase engineering (i.e. from 2H to 1T or 1T[′]) is a known route for enhancing charge transfer kinetics and improving the HER performance of TMDs [114]. Sun *et al* have investigated the HER performance of MoS₂ nanosheets with mixed phases [116] using SECM SG/TC mode (figure 8(g)). The high-resolution EC maps in figures 8(h) and (i) demonstrate that the HER activity of the 1T phase is more active compared to the 2H basal plane, while 2H-MoS₂ edges also exhibit considerable activity.

While MoS₂ is the most studied compound, other non-precious metal TMDs have also been explored. Jasion *et al* synthesized 2D FeS₂ with controlled morphology [134]. The SECM GC experiments suggested that 2D FeS₂ discs exhibit excellent HER activity and stability that is comparable to Pt.

4.3. Photoelectrochemistry

Isolating single or a few layers of TMDs from their bulk form results in fundamentally distinctive physical properties that in turn impact the photoelectrochemical behavior [135]. Both light absorption and diffusion mechanisms of charge carriers are strongly dependent on the number of layers [136].

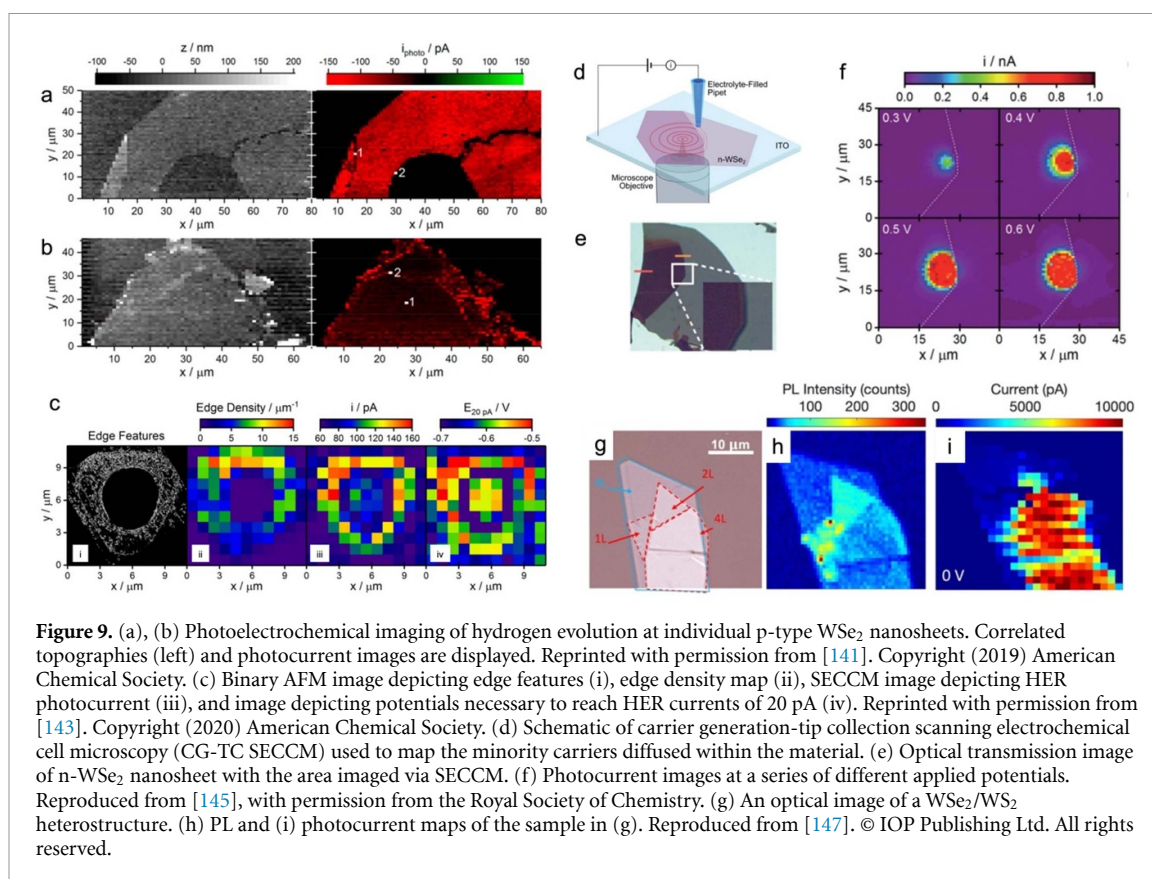


Figure 9. (a), (b) Photoelectrochemical imaging of hydrogen evolution at individual p-type WSe₂ nanosheets. Correlated topographies (left) and photocurrent images are displayed. Reprinted with permission from [141]. Copyright (2019) American Chemical Society. (c) Binary AFM image depicting edge features (i), edge density map (ii), SECCM image depicting HER photocurrent (iii), and image depicting potentials necessary to reach HER currents of 20 pA (iv). Reprinted with permission from [143]. Copyright (2020) American Chemical Society. (d) Schematic of carrier generation-tip collection scanning electrochemical cell microscopy (CG-TC SECCM) used to map the minority carriers diffused within the material. (e) Optical transmission image of n-WSe₂ nanosheet with the area imaged via SECCM. (f) Photocurrent images at a series of different applied potentials. Reproduced from [145], with permission from the Royal Society of Chemistry. (g) An optical image of a WSe₂/WS₂ heterostructure. (h) PL and (i) photocurrent maps of the sample in (g). Reproduced from [147]. © IOP Publishing Ltd. All rights reserved.

The steps/edges at the 2D TMDs in the photoelectrochemical reactions can be both beneficial and detrimental since they concurrently serve as catalytic active sites and charge recombination sites [137]. To obtain direct experimental insights into these effects requires spatially resolved characterization techniques. Scanning photocurrent microscopy using a near-filed laser scanned over the sample surface while recording the photocurrent has been employed to investigate TMDs [138–140]. However, the collected signals are inevitably affected by non-illuminated spots, and the spatial resolution is fundamentally limited by optical diffraction. Scanning EC probe techniques are free from these limitations and have seen a growing number of applications to investigate several key factors of the 2D photoelectrochemistry.

4.3.1. Defects

Hill *et al* have investigated the photoelectrochemical behavior of individual p-type WSe₂ nanosheets using SECCM [141], highlighting the effects of layer thickness and geometric defect. SECCM data of HER at p-type WSe₂ nanosheets consisting of a topographical map and photocurrent map (figures 9(a) and (b)) suggest a strong correlation between photoelectrochemical activity and structural features. Small steps were found to enhance HER photocurrents due to their high catalytic activities (spot 2 in figure 9(b)), whereas large steps were generally found to be detrimental to HER (spot 1 in figure 9(a)). This behavior was explained as due to increased charge

recombination at defect-rich sites, which degrades the photochemical response, unless the features are much smaller than the optical penetration depth [142].

SECCM was further employed to create local hole-like defects at the basal planes of individual p-type WSe₂ nanosheets by controlled anodization of the WSe₂ [143]. The defect density was mapped by AFM (figure 9(c) i, ii) and compared to correlated SECCM images (figure 9(c) iii, iv). These results provide direct evidence supporting that the increased density of monolayer-high step-like features enhances the photoelectrochemical activities of TMDs. Strange *et al* investigated the modulation of the photoluminescence (PL) of 2D MoS₂ upon EC anodization [144]. The enhancement and red-shift of the PL were originated from Mo oxidation that hinders nonradiative decay of excitons. SECCM mapping was used to reveal that the MoS₂ photooxidation is strongly localized at defective edge sites containing an abundance of Mo–SH functional groups.

4.3.2. Carrier transport

Understanding the factors governing carrier generation (CG) and transport within 2D TMDs during photoelectrochemical reactions is needed to guide the rational design of improved devices. Hill *et al* applied CG-TC SECCM to visualize carrier transport [145]. In this approach, carriers are locally generated using a focused light source and detected as they drive photoelectrochemical reactions at a spatially offset electrolyte interface (figure 9(d)). Photocurrent

Table 2. Summary of scanning electrochemical studies of TMDs.

Technique/mode	Materials	Reactions	References
SECM feedback	CVD MoS ₂	DmFc ^{+/0} , Fc ^{+/0}	[75]
SECM feedback	Exfoliated MoS ₂	Fe(CN) ₆ ^{3-/4-} , Ru(NH ₃) ₆ ^{3+/2+}	[112]
SECM tunneling mode	Solution-exfoliated 1T/1T', 2H MoS ₂ flake	FcMeOH ^{+/0} , Fe(CN) ₆ ^{3-/4-}	[115]
SECM feedback and SG/TC	Solution-exfoliated 1T, 2H MoS ₂	FcMeOH ^{+/0} , HER	[116]
SECM feedback	n-type doped 2H and 1T' CVD MoS ₂	FcMeOH ^{0/+}	[117]
SECCM hopping mode	Mechanically exfoliated MoS ₂ , WS ₂ , MoSe ₂ , WSe ₂	Ru(NH ₃) ₆ ^{3+/2+}	[118]
SECCM hopping mode	Mechanically exfoliated MoS ₂ , MoSe ₂ , WSe ₂ on Au	Ru(NH ₃) ₆ ^{3+/2+}	[113]
AFM-SECM feedback	CVD MoS ₂	DmFc ^{+/0} , Fc ^{+/0}	[119]
SECCM, single-channel pipette	Mechanically exfoliated MoS ₂	FcMeOH ^{+/0} , Ru(NH ₃) ₆ ^{3+/2+}	[120]
SECCM hopping mode	Cleaved MoS ₂ crystal	HER	[43]
SECCM hopping mode	Cleaved MoS ₂ , WS ₂ crystal	HER	[128]
SECCM hopping mode	1H-MoS ₂ , MoS ₂ /WS ₂	HER	[131]
SECM SG/TC	CVD monolayer 2H-MoS ₂	HER	[133]
SECM SG/TC	Solution-processing synthesized FeS ₂ discs	HER	[134]
SECCM hopping mode	Mechanically exfoliated p-type WSe ₂	Ru(NH ₃) ₆ ^{3+/2+} , HER	[141]
SECCM hopping mode	Mechanically exfoliated p-type WSe ₂	HER, anodization of WSe ₂	[143]
SECCM carrier generation-tip collection	Mechanically exfoliated n-type WSe ₂	I ₂ /I ⁻	[145]
SECCM-PL	Mechanically exfoliated WS ₂ , p-type WSe ₂ , WSe ₂ /WS ₂	I ₂ /I ⁻	[147]
SECCM-PL	CVD MoS ₂	Oxidation of MoS ₂	[144]
SECCM carrier generation-tip collection	Mechanically exfoliated n-type WSe ₂	I ₂ /I ⁻	[146]
SECCM hopping mode	n-type MoS ₂ /p-type Cu ₂ O	HER	[149]
SECCM hopping mode	CVD monolayer 2H-MoS ₂ on GC	HER	[150]
SECCM hopping mode	CVD monolayer 2H-MoS ₂ on GC	HER	[151]

images of an n-WSe₂ nanosheet (figure 9(e)) showed photocurrents increased in magnitude and widened spatially with increasing potential. Photocurrents at the edge (indicated by the dashed line) were significantly reduced, providing a clear, unambiguous visualization of carrier recombination at nanoscale defects (figure 9(f)). Tolbert *et al* extended the CG-TC SECCM approach to probe exciton transport down to monolayer limit [146]. Photogenerated excitons in monolayer WSe₂ were found to drive reactions across distances in excess of 20 μm, suggesting the existence of long-lived charge transfer states.

4.3.3. Heterostructure assembly

Van der Waals heterojunctions formed by stacking different TMD monolayers or multilayers enable possibilities to create novel p-n junctions at the atomic scale for energy-harvesting applications [148]. Fu *et al* combined SECCM with PL to investigate the layer-dependence of photocurrents in WSe₂/WS₂ vertical heterostructures [147]. Figures 9(g)–(i) showed reduced PL intensity in the heterojunction region compared with pristine monolayer WSe₂, while the highest photocurrent was detected in the 4L WSe₂/4L

WS₂ location. The reduction of PL and enhancement of photocurrent is mainly due to enhanced charge transfer and exciton dissociation in the heterojunction. Importantly, the photocurrent in WSe₂/WS₂ heterostructures increases with the increasing thickness of WSe₂. Zheng *et al* examined the performance of MoS₂/Cu₂O nanorod-arrays heterostructures in photoelectrochemical HER [149]. SECCM maps showed higher photocurrent at strained heterostructures, in which strain was applied by controlling the height of the Cu₂O nanorods. The results indicated that a more efficient separation of photogenerated carriers induced by the strain can effectively enhance HER activity.

In table 2 we summarize SECM/SECCM work on 2D TMD related materials. In analogous to graphene, the structural effects such as edge, defects, and thickness on HET and electrocatalytic reactions at TMDs have been shown to be impactful. In addition, spatially resolved measurements have elucidated the roles of phase, atomic vacancies, and strains in regulating the reactivity of TMD layers. Coupled with electromagnetic excitation, insights into the dynamics of carrier transport and the implications in

photoelectrochemistry were obtained from SECCM images.

5. Transition metal oxides (TMOs), hydroxides (TMHs), nitrides, and carbides

5.1. Transition metal oxides and hydroxides (TMOs and TMHs)

Most pristine TMOs and TMHs exhibit unsatisfactory performance in their bulk forms due to their poor activity and conductivity. The electrocatalytic activity of TMOs and TMHs can be significantly improved by shrinking their size and reducing the thickness towards the atomic scale [8]. Two-dimensional (2D) TMOs and TMHs are especially active for electrocatalytic reactions involving the activation of water such as the oxygen evolution reaction (OER) [152, 153]. Nanoscale SECM and SECCM have been shown to be powerful *operando* techniques for accurately correlating the electrocatalytic OER activities with the local structures.

5.1.1. Defects

Through defect engineering, the OER activity of faceted nickel oxide (NiO) nanostructures was enhanced due to the exposure of nanoscale edge sites that significantly alter the electronic structure of Ni²⁺ centers and promoted Ni³⁺ states [154]. Sun *et al* employed SECM to probe 2D NiO nanosheets containing defect holes with well-defined edges, and directly correlated the electrocatalytic OER activities with the local structural defects [155]. The tip electrode collects the oxygen generated at the substrate in SG/TC mode (figure 10(a)). The SECM image in figure 10(b) shows more efficient O₂ generation at the NiO surface compared to the inactive HOPG. The map with even higher resolution shows increased OER current at the NiO/HOPG boundary (figure 10(c)), consistent with a significantly higher activity of the NiO edge. Atomic-resolution structural measurements of the edges using electron tomography showed that the edges are terminated with (100) and (111) facets, which were responsible for ~200-fold enhancement of activity.

5.1.2. Ion insertion

Ion insertion redox reactions convert inactive materials into active electrocatalysts during operation. Single-crystalline β -Co(OH)₂ catalyzed OER is accompanied by hydroxide, water, and proton (de)intercalation as well as the change in the oxidation state of cobalt. Mefford *et al* used a suite of correlative SECCM and x-ray microscopy techniques [156] to establish a link between the OER activity and the local structure of β -Co(OH)₂. Importantly, direct mapping of the OER current with SECCM (figure 10(d)) revealed that edge facets are the active surfaces. In both scanning mode (figure 10(e)) and hopping mode (figure 10(f)), the SECCM images

revealed that the edge facets have high EC activity compared with the low activity of the basal planes. The difference of these facets was rationalized by the ion (de)intercalation characteristics of the system, in which ion (de)intercalation is facilitated at the edge facets, while ion movement is restricted in the absence of extended defects, which prevents the basal planes from serving as reaction sites.

5.2. MXenes

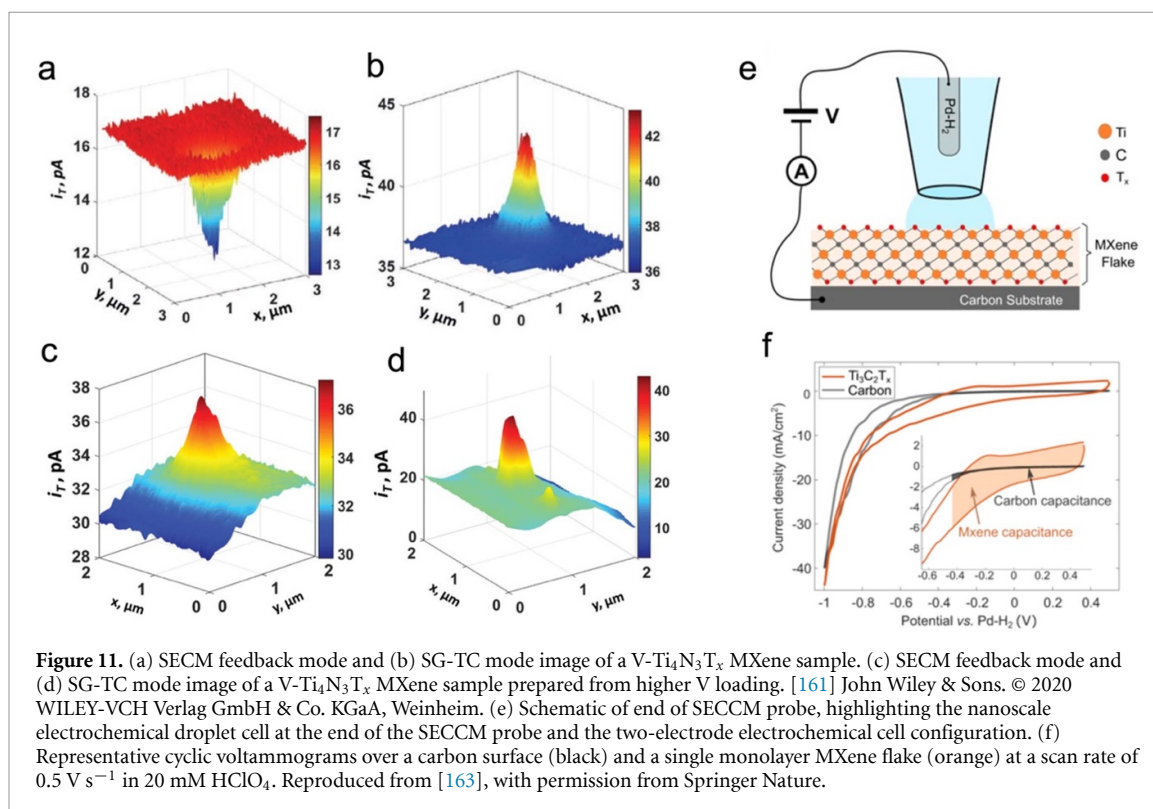
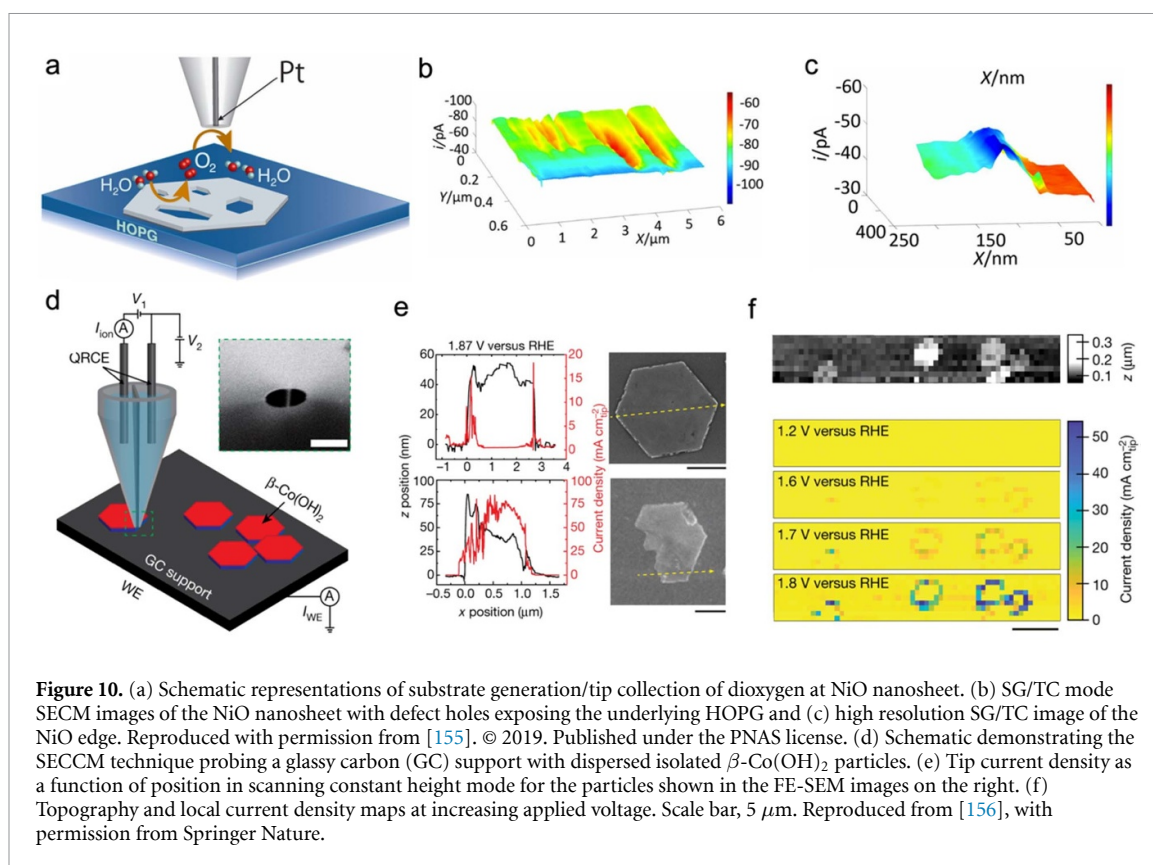
MXenes are a class of 2D materials consisting of layers of transition metal carbides, nitrides, or carbonitrides [157]. The versatile chemistry of MXenes leads to tunable properties for applications including energy storage, sensors, and catalysis [158, 159]. The general formula of MXenes is M_{n+1}X_nT_x, where M is an early transition metal, X is carbon and/or nitrogen, and T is a functional group. Metallic MXenes that possess inherently active basal planes have been investigated via scanning EC approaches.

5.2.1. Conductivity

Gupta *et al* employed SECM to quantify the HET kinetics of Fe(CN)₆^{4-/3-} at Ti₃C₂T_x MXenes and discovered a strong dependence on flake thickness and the type of electrolyte [160]. Djire *et al* have developed mixed transition metal nitride MXenes and investigated their HER catalytic activity with SECM [161]. Specifically, SECM was employed to determine the conductivity and catalytic activity of individual V-Ti₄N₃T_x nanoflakes. The feedback map shown in figure 11(a) using Fc as the redox mediator exhibits no measurable redox regeneration, while the SG-TC map in an acidic solution shows measurable activity toward HER (figure 11(b)). The SECM results were explained by proposing that the basal planes of these V-Ti₄N₃T_x are catalytically active despite their limited conductivity, due to the large exposed metallic sites available for proton adsorption. However, we note that modification of the conductivity and EC behavior by H⁺ adsorption or intercalation [162] could be an alternative explanation for this apparent contradictory behavior. By increasing the V loading, enhanced conductivity and metallic character were observed in the feedback and SG-TC maps (figures 11(c) and (d)).

5.2.2. Charge storage mechanism

Titanium carbide MXenes exhibit excellent performance as supercapacitors, with a charge storage mechanism associated with fast ion intercalation into the interlayer space. Cabre *et al* conducted an SECCM study [163] to analyze a small subregion of a monolayer Ti₃C₂T_x flake where contributions from ion-intercalation processes were eliminated, allowing them to isolate surface-dependent processes that contribute to MXene pseudocapacitive response. Using an SECCM approach, cyclic voltammograms (figures 11(e) and (f)) and quantitative analysis of



the pseudocapacitive response revealed that entire MXene flakes were charged through EC contact of only a small basal plane subregion, corresponding to as little as 3% of the surface area. These results suggest that the proton transport across the surface acts

as a complementary mechanism during the fast charging/discharging of MXene-based supercapacitors.

In table 3 we summarize SECM/SECCM work on 2D TMO, TMH, and MXenes. Unique insights into the roles of structural heterogeneities were gained

Table 3. Summary of scanning electrochemical studies of TMOs and MXenes.

Technique/mode	Materials	Reactions	References
SECM feedback and SG/TC	NiO nanosheet	OER, FcMeOH ^{+ /0}	[155]
SECCM hopping mode	β -CO(OH) ₂	OER	[156]
SECM feedback	Ti ₃ C ₂ T _x flakes	Fe(CN) ₆ ^{4- /3-}	[160]
SECM feedback and SG/TC	M-Ti ₄ N ₃ T _x (M = V, Cr, Mo, Mn)	FcMeOH ^{+ /0} , HER	[161]
SECCM hopping mode	Ti ₃ C ₂ T _x flakes	Pseudocapacitive processes in HER	[163]

through SECM/SECCM and correlative characterization techniques. We also note the benefits of the versatile SECM in understanding the correlation between conductivity and reactivity, as well as the capability of SECCM in selectively probing specific sites to clarify charge storage mechanisms.

6. Conclusions and perspectives

In this review, we have highlighted the development of scanning EC probe approaches to address questions related to the (photo)electrochemistry of 2D materials that are inscrutable using conventional methods. Experimental conditions of these research efforts have been outlined in tables 1–3. Versatile scanning EC platforms have proven to be capable of resolving EC information with a high spatial resolution to understand the structure–function relationships of the electroactive 2D materials.

6.1. Advantages and limitations

The most advantageous qualities of SECM/SECCM are originated from the miniaturization of the EC probes. Specifically, the high-resolution EC mapping has been shown to be effective in identifying heterogeneities that are buried in ensemble measurements, providing a general strategy to visualize the activity variation across the surface of a 2D material. As a result, the effects of morphology, defects, dopants, strain, substrate, and other factors are readily examined. Other benefits include (1) these non-destructive approaches allow the materials to be studied without altering their intrinsic properties; (2) the 2D material samples are not required to be manufactured into a device format; (3) the (micro)nano scale measurements reduce the background and improve the signal-to-noise ratio; (4) the ability to detect and quantify intermediates provides unique insights into reaction mechanisms; (5) both *in-situ* and *ex-situ* spectroscopic/microscopic analysis can be coupled to correlate activities with physical properties.

In comparison to other EC techniques, SECM/SECCM presents distinct advantages. Ensemble measurements using a conventional three-electrode setup fall short in resolving local variations. While integrating individual 2D flakes into on-chip devices [16, 164] allows for local EC interrogation, its spatial resolution typically remains confined to micrometer scales. It is important to note that polymer contamination from the photoresist often proves

unavoidable, undermining measurement reliability. Microdroplet techniques [60, 111] bear conceptual similarities to SECCM, yet their throughput is constrained as only a small fraction of the 2D material can be probed at any given time. EC–STM [165] or EC–AFM [166] enables real-time observation of nanoscale surface morphology changes but is constrained by its inability to capture potential-dependent images. Moreover, the close proximity of the tip may interfere with EC processes at the 2D layers, potentially inducing shielding effects and introducing inaccuracies in measurements.

Despite the high merit of SECM/SECCM in investigating the electrochemistry of 2D materials, some limitations and challenges need to be overcome to push their applications to the next level. (1) The spatial resolution of SECM is influenced by both the size of nanoelectrode tip and diffusional broadening [21]. The resolution of SECCM is determined by the size of nanopipette probe and wetting property of the sample. Strategies to push their resolution to a few nanometers or atomic scale are yet to be developed. (2) The fabrication of SECM tips can be complex and often irreproducible, while the knowledge of geometry and dimensions of the probes is crucial for reliable quantitative data analysis. (3) Both high-resolution SECCM and SECCM mapping experiments are time-consuming. This limitation demands high instrument stability that needs to be engineered through environmental control (e.g. vibrational isolation and humidity control). The poor temporal resolution limits studies of rapid dynamic EC processes. (4) Electroanalytical techniques (e.g. voltammetry, amperometry, and impedance spectroscopy) integrated in SECM/SECCM alone are incapable of providing comprehensive chemical information in complex catalytic reactions, limiting the ability to characterize intermediates/products distribution and reaction mechanisms.

6.2. Perspectives on technique development

The intuitive approaches to improve the spatial resolution of SECM/SECCM are probe miniaturization down to nanometers. While this is attractive, one should account for the changes of the fundamental behavior of nanoprobe associated with the shrink of size. Drastic double layer effects can impact the migration of redox ions that leads to either enhancement or inhibition to faradaic current [167]. As a result, factors including electrolyte concentration,

solvent dielectric property, and surface charge needs to be considered. Careful characterization of nano-electrodes and nanopipettes is critical because unambiguous geometric parameters of the probes are necessary to interpret data. In SECCM, the true electroactive area is estimated by characterizing the meniscus ‘footprint’ with other microscopies [29]. Consequently, the surface chemistry of probed materials and the polarity of the solvent should be considered to control the meniscus contact. Further discussions on probe fabrication and characterization can be found elsewhere [22, 32, 33, 168]. Alternative approaches to improve the spatial resolution other than probe engineering have been developed based on data postprocessing [27, 169]. For instance, algorithms to produce point spread function corrected SECM image have been developed to relax the requirement of small probes [170].

Reproducibility in SECM and SECCM may be impacted by fluctuations in probe geometry and surface hydrophobicity. As discussed earlier, meticulous characterization of probes is essential for ensuring dependable measurements. Surface modification of an SECCM probe, often achieved through silanization [171] of the glass nanopipette’s outer walls with hydrophobic or hydrophilic groups, can bolster the stability of meniscus contact. An alternative approach, oil-immersed scanning micropipette contact method [172] improves droplet stability, particularly beneficial for aqueous solutions susceptible to evaporation in uncontrolled humidity environments.

Environmental variables like temperature and humidity can introduce variability in repeated measurements. Maintaining stable humidity levels is crucial for consistent SECCM measurements, achievable through humidified gas streams or humidifiers. Recent advancements involve integrating SECCM setups into glovebox environments [173], heightening precision when examining moisture and oxygen-sensitive materials.

Slow imaging speed remains as main challenge in SECM/SECCM mapping measurements. Developing new scanning patterns [174] and fluid dynamic simulations [175] to aid high-speed scanning have shown immense potential for applications in large data acquisition. We also envision that implementing artificial intelligence driven automation [176, 177] will find a niche in scanning probe electrochemistry. In methods as such, self-driving experiments enabled by artificial intelligence are performed to identify and measure representative data in lieu of full dataset [176], therefore promoting the efficiency of measurements. However, this algorithm may not apply to complex EC systems with heterogeneities, and careful verification of the data fidelity is required.

Integrating SECM/SECCM with complementary techniques [178] is another promising avenue to pursue the comprehensive characterization of 2D

materials. Combining *in-situ* Raman spectroscopy [15] and SECM/SECCM is expected to provide vital information on the evolution of structure, charge density, and surface chemistry of the 2D electrode during a reaction, although matching the optical resolution with that of SECM/SECCM and eliminating the interference from probe tips remain challenging. Coupling scanning EC probes to mass spectrometers [179] would allow researcher to extract spatially resolved product distribution in complex reactions such as CO₂ catalysis and EC organic synthesis. Challenges in achieving sufficient sensitivity to detect chemistry taking place at the nano- or micron-sized interfaces should be noted. Fabricating 2D materials in a field-effect transistor configuration [120, 180] is particularly promising in measuring/controlling the electronic transport in a 2D layer while it is interrogated with SECM/SECCM. Multifunctional analytical platforms such as these would tremendously expand the versatility of scanning EC probe techniques and make them even more suited to investigating the rich physics and chemistry of 2D materials.

6.3. Perspectives on future objectives

There remains a wide space to expand the availability of SECM/SECCM to explore the untapped domains of 2D materials. While the studies described in this review are mostly devoted to revealing the activities of structural features, a wide variety of additional strategies to activate the inert pristine surfaces of 2D layers remain to be explored. For instance, the modulation of electronic structure by means of ion intercalation [181, 182], external field effects [183–185] and other ‘quantum’ engineering [186] approaches are expected to impact the HET kinetics and catalytic activities. In addition to the reactions covered in this review, 2D materials have been shown to support other important reactions such as CO₂ reduction and ammonia synthesis. The complicated reaction mechanisms of CO₂ reduction [187, 188] and nitrogen fixation [189] are largely hypothesized without direct experimental detection of intermediates. The opportunities for SECM/SECCM include using high-resolution mapping to identify catalytic active sites and adopting the nanogap methods [190, 191] to detect intermediates that can elucidate the complex mechanisms of these multi-electron, multi-proton reactions at the 2D catalysts. The chemical stability of the materials themselves requires attention as 2D catalysts undergo different degrees of corrosion [192] while mediating interfacial chemical transformations.

Many more materials and derivatives in the existing library of 2D crystals deserve attention. For instance, black phosphorus [193] is a layered semiconductor with distinctive properties for applications in energy storage and catalysis [194]. Two-dimensional (2D) analogues of metal–organic frameworks possess a high degree of exposed catalytic active

sites and tunable structures that are also suitable for the synthesis of single-atom catalysts with high reported electrocatalytic activities [195]. The versatility and tunability of 2D materials may be further enhanced by fabricating vdW heterostructures [25, 196–199] formed with dissimilar 2D layers. The new chemistry produced by constructing distinctive vdW heterointerfaces awaits rigorous investigation with nanoscale EC microscopy.

The capability of SECM and SECCM renders them indispensable in sensor technology and energy storage. SECM/SECCM enhances sensor design by enabling precise mapping of EC activity on sensor surfaces, crucial for crafting highly sensitive and selective sensing platforms catering to a myriad of analytes, from small molecules to biomolecules [200, 201]. The growing application of 2D materials in sensors is propelled by their distinctive attributes including a high surface-area-to-volume ratio, abundant reactive sites, and mechanical resilience and flexibility, aligning seamlessly with cutting-edge technologies like wearable electronics [202]. We foresee exciting prospects in amalgamating SECM/SECCM with the developmental trajectory of 2D materials in sensor innovation. Both SECM and SECCM offer avenues to scrutinize the formation of SEIs on electrodes—a pivotal facet of battery research [203]. Furthermore, by unraveling multiple charge transfer and mass transfer mechanisms in the complex EC systems, SECM/SECCM can directly impact the evolution of more efficient metal-ion batteries [203, 204]. The suitability of 2D materials as advanced battery electrode materials stems from their expansive specific surface area, minimized ion diffusion distances, and capacity to mitigate volume fluctuations during repeated charge/discharge cycles [205, 206]. The convergence of SECM/SECCM with the evolution of 2D materials for energy storage applications holds great promise.

In summary, scanning EC probe techniques have shown immense potential to become some of the most powerful tools for the characterization of 2D materials. Continued collaborations among chemists, physicists, and materials scientists will realize the next generation of high throughput EC microscopy and accelerate the discovery of exciting phenomena in this unique family of materials.

Data availability statement

No new data were created or analyzed in this study.

Acknowledgments

This material is in part based upon work supported by the US Department of Energy, Office of Science, Office of Basic Energy Sciences, under Award No. DE-SC0021049 (K.Z., S.M., D.K.B.). This work was also funded in part by 4-VA, a collaborative partnership

for advancing the Commonwealth of Virginia (P.A., J.R.J., Y.Y.). Y.Y. also acknowledges support from the George Mason University Quantum Science and Engineering Center.

Conflict of interest

There are no conflicts to declare.

ORCID iDs

Kaidi Zhang  <https://orcid.org/0000-0002-1453-0681>

Kwabena Bediako  <https://orcid.org/0000-0003-0064-9814>

Yun Yu  <https://orcid.org/0000-0002-0204-1012>

References

- [1] Sangwan V K and Hersam M C 2018 Electronic transport in two-dimensional materials *Annu. Rev. Phys. Chem.* **69** 299–325
- [2] Tan C *et al* 2017 Recent advances in ultrathin two-dimensional nanomaterials *Chem. Rev.* **117** 6225–331
- [3] Zeng M, Xiao Y, Liu J, Yang K and Fu L 2018 Exploring two-dimensional materials toward the next-generation circuits: from monomer design to assembly control *Chem. Rev.* **118** 6236–96
- [4] Pham P V, Bodepudi S C, Shehzad K, Liu Y, Xu Y, Yu B and Duan X 2022 2D heterostructures for ubiquitous electronics and optoelectronics: principles, opportunities, and challenges *Chem. Rev.* **122** 6514–613
- [5] Hess P 2021 Bonding, structure, and mechanical stability of 2D materials: the predictive power of the periodic table *Nanoscale Horiz.* **6** 856–92
- [6] Turunen M, Brotons-Gisbert M, Dai Y, Wang Y, Scerri E, Bonato C, Jöns K D, Sun Z and Gerardot B D 2022 Quantum photonics with layered 2D materials *Nat. Rev. Phys.* **4** 219–36
- [7] Deng D, Novoselov K S, Fu Q, Zheng N, Tian Z and Bao X 2016 Catalysis with two-dimensional materials and their heterostructures *Nat. Nanotechnol.* **11** 218–30
- [8] Jin H, Guo C, Liu X, Liu J, Vasileff A, Jiao Y, Zheng Y and Qiao S-Z 2018 Emerging two-dimensional nanomaterials for electrocatalysis *Chem. Rev.* **118** 6337–408
- [9] Mendes R G, Pang J, Bachmatiuk A, Ta H Q, Zhao L, Gemming T, Fu L, Liu Z and Rümmler M H 2019 Electron-driven in situ transmission electron microscopy of 2D transition metal dichalcogenides and their 2D heterostructures *ACS Nano* **13** 978–95
- [10] Luo C, Wang C, Wu X, Zhang J and Chu J 2017 In situ transmission electron microscopy characterization and manipulation of two-dimensional layered materials beyond graphene *Small* **13** 1604259
- [11] van Oversteeg C H M, Doan H Q, de Groot F M F and Cuk T 2017 In situ x-ray absorption spectroscopy of transition metal based water oxidation catalysts *Chem. Soc. Rev.* **46** 102–25
- [12] Pacilé D, Papagno M, Rodríguez A F, Grioni M, Papagno L, Girit Ç Ö, Meyer J C, Begtrup G E and Zettl A 2008 Near-edge x-ray absorption fine-structure investigation of graphene *Phys. Rev. Lett.* **101** 066806
- [13] Ferrari A C and Basko D M 2013 Raman spectroscopy as a versatile tool for studying the properties of graphene *Nat. Nanotechnol.* **8** 235–46
- [14] Paillet M, Parret R, Sauvajol J-L and Colombari P 2018 Graphene and related 2D materials: an overview of the Raman studies *J. Raman Spectrosc.* **49** 8–12

- [15] Zhang S, Zhang N, Zhao Y, Cheng T, Li X, Feng R, Xu H, Liu Z, Zhang J and Tong L 2018 Spotting the differences in two-dimensional materials—the Raman scattering perspective *Chem. Soc. Rev.* **47** 3217–40
- [16] Yang H, He Q, Liu Y, Li H, Zhang H and Zhai T 2020 On-chip electrocatalytic microdevice: an emerging platform for expanding the insight into electrochemical processes *Chem. Soc. Rev.* **49** 2916–36
- [17] Zhu X, Wang C and Fu L 2020 Engineering electrocatalytic microcells for two-dimensional materials *Cell Rep. Phys. Sci.* **1** 100190
- [18] Engstrom R C, Weber M, Wunder D J, Burgess R and Winquist S 1986 Measurements within the diffusion layer using a microelectrode probe *Anal. Chem.* **58** 844–8
- [19] Bard A J, Fan F R F, Kwak J and Lev O 1989 Scanning electrochemical microscopy. Introduction and principles *Anal. Chem.* **61** 132–8
- [20] Ebejer N, Schnippering M, Colburn A W, Edwards M A and Unwin P R 2010 Localized high resolution electrochemistry and multifunctional imaging: scanning electrochemical cell microscopy *Anal. Chem.* **82** 9141–5
- [21] Ebejer N, Güell A G, Lai S C S, McKelvey K, Snowden M E and Unwin P R 2013 Scanning electrochemical cell microscopy: a versatile technique for nanoscale electrochemistry and functional imaging *Annu. Rev. Anal. Chem.* **6** 329–51
- [22] Polcari D, Dauphin-Ducharme P and Mauzeroll J 2016 Scanning electrochemical microscopy: a comprehensive review of experimental parameters from 1989 to 2015 *Chem. Rev.* **116** 13234–78
- [23] Xu X, Valavanis D, Ciocci P, Confederat S, Marcuccio F, Lemineur J-F, Actis P, Kanoufi F and Unwin P R 2023 The new era of high-throughput nanoelectrochemistry *Anal. Chem.* **95** 319–56
- [24] Bard A J and Mirkin M V 2012 *Scanning Electrochemical Microscopy* 2nd edn (CRC Press)
- [25] Velický M and Toth P S 2017 From two-dimensional materials to their heterostructures: an electrochemist's perspective *Appl. Mater. Today* **8** 68–103
- [26] Jaouen K, Henrotte O, Campidelli S, Josselme B, Derycke V and Cornut R 2017 Localized electrochemistry for the investigation and the modification of 2D materials *Appl. Mater. Today* **8** 116–24
- [27] Mishra A, Sarbapalli D, Rodríguez O and Rodríguez-López J 2023 Electrochemical imaging of interfaces in energy storage via scanning probe methods: techniques, applications, and prospects *Annu. Rev. Anal. Chem.* **16** 93–115
- [28] Santana Santos C, Jaato B N, Sanjuán I, Schuhmann W and Andronescu C 2023 Operando scanning electrochemical probe microscopy during electrocatalysis *Chem. Rev.* **123** 4972–5019
- [29] Bentley C L 2022 Scanning electrochemical cell microscopy for the study of (nano)particle electrochemistry: from the sub-particle to ensemble level *Electrochem. Sci. Adv.* **2** e2100081
- [30] Bentley C L, Edmondson J, Meloni G N, Perry D, Shkirskiy V and Unwin P R 2019 Nanoscale electrochemical mapping *Anal. Chem.* **91** 84–108
- [31] Zoski C G 2002 Ultramicroelectrodes: design, fabrication, and characterization *Electroanalysis* **14** 1041–51
- [32] Perry D, Momotenko D, Lazenby R A, Kang M and Unwin P R 2016 Characterization of nanopipettes *Anal. Chem.* **88** 5523–30
- [33] Chen R, Balla R J, Lima A and Amemiya S 2017 Characterization of nanopipet-supported ITIES tips for scanning electrochemical microscopy of single solid-state nanopores *Anal. Chem.* **89** 9946–52
- [34] Lefrou C and Cornut R 2010 Analytical expressions for quantitative scanning electrochemical microscopy (SECM) *ChemPhysChem* **11** 547–56
- [35] Amemiya S, Nioradze N, Santhosh P and Deible M J 2011 Generalized theory for nanoscale voltammetric measurements of heterogeneous electron-transfer kinetics at macroscopic substrates by scanning electrochemical microscopy *Anal. Chem.* **83** 5928–35
- [36] Azevedo J, Fillaud L, Bourdillon C, Noël J-M, Kanoufi F, Josselme B, Derycke V, Campidelli S and Cornut R 2014 Localized reduction of graphene oxide by electrogenerated naphthalene radical anions and subsequent diazonium electrografting *J. Am. Chem. Soc.* **136** 4833–6
- [37] Macpherson J V and Unwin P R 2000 Combined scanning electrochemical—atomic force microscopy *Anal. Chem.* **72** 276–85
- [38] Kranz C, Friedbacher G, Mizaikoff B, Lugstein A, Smoliner J and Bertagnoli E 2001 Integrating an ultramicroelectrode in an AFM cantilever: combined technology for enhanced information *Anal. Chem.* **73** 2491–500
- [39] Comstock D J, Elam J W, Pellin M J and Hersam M C 2010 Integrated ultramicroelectrode—nanopipet probe for concurrent scanning electrochemical microscopy and scanning ion conductance microscopy *Anal. Chem.* **82** 1270–6
- [40] Takahashi Y, Shevchuk A I, Novak P, Murakami Y, Shiku H, Korchev Y E and Matsue T 2010 Simultaneous noncontact topography and electrochemical imaging by SECM/SICM featuring ion current feedback regulation *J. Am. Chem. Soc.* **132** 10118–26
- [41] Bard A J 2010 Inner-sphere heterogeneous electrode reactions. Electrocatalysis and photocatalysis: the challenge *J. Am. Chem. Soc.* **132** 7559–67
- [42] Bentley C L, Kang M and Unwin P R 2019 Nanoscale surface structure—activity in electrochemistry and electrocatalysis *J. Am. Chem. Soc.* **141** 2179–93
- [43] Bentley C L, Kang M and Unwin P R 2017 Nanoscale structure dynamics within electrocatalytic materials *J. Am. Chem. Soc.* **139** 16813–21
- [44] Williams C G, Edwards M A, Colley A L, Macpherson J V and Unwin P R 2009 Scanning micropipet contact method for high-resolution imaging of electrode surface redox activity *Anal. Chem.* **81** 2486–95
- [45] Novoselov K S, Geim A K, Morozov S V, Jiang D, Zhang Y, Dubonos S V, Grigorieva I V and Firsov A A 2004 Electric field effect in atomically thin carbon films *Science* **306** 666–9
- [46] Zhang Y, Tan Y-W, Stormer H L and Kim P 2005 Experimental observation of the quantum Hall effect and Berry's phase in graphene *Nature* **438** 201–4
- [47] Kaplan A, Yuan Z, Benck J D, Govind Rajan A, Chu X S, Wang Q H and Strano M S 2017 Current and future directions in electron transfer chemistry of graphene *Chem. Soc. Rev.* **46** 4530–71
- [48] Bard A J and Faulkner L R 2001 *Electrochemical Methods: Fundamentals and Applications* 2nd edn (Wiley)
- [49] Li W, Tan C, Lowe M A, Abruña H D and Ralph D C 2011 Electrochemistry of individual monolayer graphene sheets *ACS Nano* **5** 2264–70
- [50] Ritzert N L, Rodríguez-López J, Tan C and Abruña H D 2013 Kinetics of interfacial electron transfer at single-layer graphene electrodes in aqueous and nonaqueous solutions *Langmuir* **29** 1683–94
- [51] Tan C, Rodríguez-López J, Parks J J, Ritzert N L, Ralph D C and Abruña H D 2012 Reactivity of monolayer chemical vapor deposited graphene imperfections studied using scanning electrochemical microscopy *ACS Nano* **6** 3070–9
- [52] Zhong J-H, Zhang J, Jin X, Liu J-Y, Li Q, Li M-H, Cai W, Wu D-Y, Zhan D and Ren B 2014 Quantitative correlation between defect density and heterogeneous electron transfer rate of single layer graphene *J. Am. Chem. Soc.* **136** 16609–17
- [53] Schorr N B, Jiang A G and Rodríguez-López J 2018 Probing graphene interfacial reactivity via simultaneous and

- colocalized Raman–scanning electrochemical microscopy imaging and interrogation *Anal. Chem.* **90** 7848–54
- [54] Lai S C S, Patel A N, McKelvey K and Unwin P R 2012 Definitive evidence for fast electron transfer at pristine basal plane graphite from high-resolution electrochemical imaging *Angew. Chem., Int. Ed.* **51** 5405–8
- [55] Velický M, Toth P S, Woods C R, Novoselov K S and Dryfe R A W 2019 Electrochemistry of the basal plane versus edge plane of graphite revisited *J. Phys. Chem. C* **123** 11677–85
- [56] Unwin P R, Güell A G and Zhang G 2016 Nanoscale electrochemistry of sp^2 carbon materials: from graphite and graphene to carbon nanotubes *Acc. Chem. Res.* **49** 2041–8
- [57] Güell A G, Ebejer N, Snowden M E, Macpherson J V and Unwin P R 2012 Structural correlations in heterogeneous electron transfer at monolayer and multilayer graphene electrodes *J. Am. Chem. Soc.* **134** 7258–61
- [58] Güell A G, Cuharuc A S, Kim Y-R, Zhang G, Tan S-Y, Ebejer N and Unwin P R 2015 Redox-dependent spatially resolved electrochemistry at graphene and graphite step edges *ACS Nano* **9** 3558–71
- [59] Toth P S, Valota A T, Velický M, Kinloch I A, Novoselov K S, Hill E W and Dryfe R A W 2014 Electrochemistry in a drop: a study of the electrochemical behaviour of mechanically exfoliated graphene on photoresist coated silicon substrate *Chem. Sci.* **5** 582–9
- [60] Velický M et al 2014 Electron transfer kinetics on mono- and multilayer graphene *ACS Nano* **8** 10089–100
- [61] Rapino S, Treossi E, Palermo V, Marcaccio M, Paolucci F and Zerbetto F 2014 Playing peekaboo with graphene oxide: a scanning electrochemical microscopy investigation *Chem. Commun.* **50** 13117–20
- [62] Hui J, Zhou X, Bhargava R, Chinderle A, Zhang J and Rodríguez-López J 2016 Kinetic modulation of outer-sphere electron transfer reactions on graphene electrode with a sub-surface metal substrate *Electrochim. Acta* **211** 1016–23
- [63] Liu D-Q et al 2021 Adiabatic versus non-adiabatic electron transfer at 2D electrode materials *Nat. Commun.* **12** 7110
- [64] Chen R, Nioradze N, Santhosh P, Li Z, Surwade S P, Shenoy G J, Parobek D G, Kim M A, Liu H and Amemiya S 2015 Ultrafast electron transfer kinetics of graphene grown by chemical vapor deposition *Angew. Chem., Int. Ed.* **54** 15134–7
- [65] Cao Y, Fatemi V, Fang S, Watanabe K, Taniguchi T, Kaxiras E and Jarillo-Herrero P 2018 Unconventional superconductivity in magic-angle graphene superlattices *Nature* **556** 43–50
- [66] Yu Y et al 2022 Tunable angle-dependent electrochemistry at twisted bilayer graphene with moiré flat bands *Nat. Chem.* **14** 267–73
- [67] Kazmierczak N P, Van Winkle M, Ophus C, Bustillo K C, Carr S, Brown H G, Ciston J, Taniguchi T, Watanabe K and Bediako D K 2021 Strain fields in twisted bilayer graphene *Nat. Mater.* **20** 956–63
- [68] Van Winkle M et al 2023 Rotational and dilational reconstruction in transition metal dichalcogenide moiré bilayers *Nat. Commun.* **14** 2989
- [69] Zhang K et al 2023 Anomalous interfacial electron-transfer kinetics in twisted trilayer graphene caused by layer-specific localization *ACS Cent. Sci.* **9** 1119–28
- [70] Xu R, Guo J, Mi S, Wen H, Pang F, Ji W and Cheng Z 2022 Advanced atomic force microscopies and their applications in two-dimensional materials: a review *Mater. Futures* **1** 032302
- [71] Rojaee R and Shahbazian-Yassar R 2020 Two-dimensional materials to address the lithium battery challenges *ACS Nano* **14** 2628–58
- [72] Whittingham M S 2014 Ultimate limits to intercalation reactions for lithium batteries *Chem. Rev.* **114** 11414–43
- [73] Azevedo J, Bourdillon C, Derycke V, Campidelli S, Lefrou C and Cornut R 2013 Contactless surface conductivity mapping of graphene oxide thin films deposited on glass with scanning electrochemical microscopy *Anal. Chem.* **85** 1812–8
- [74] Bourgeteau T, Le Vot S, Bertucchi M, Derycke V, Jousset B, Campidelli S and Cornut R 2014 New insights into the electronic transport of reduced graphene oxide using scanning electrochemical microscopy *J. Phys. Chem. Lett.* **5** 4162–6
- [75] Henrotte O, Bottein T, Casademont H, Jaouen K, Bourgeteau T, Campidelli S, Derycke V, Jousset B and Cornut R 2017 Electronic transport of MoS_2 monolayered flakes investigated by scanning electrochemical microscopy *ChemPhysChem* **18** 2777–81
- [76] Jin R, Lu H-Y, Cheng L, Zhuang J, Jiang D and Chen H-Y 2022 Highly spatial imaging of electrochemical activity on the wrinkles of graphene using all-solid scanning electrochemical cell microscopy *Fundam. Res.* **2** 193–7
- [77] Bentley C L, Kang M, Bukola S, Creager S E and Unwin P R 2022 High-resolution ion-flux imaging of proton transport through graphene|nafion membranes *ACS Nano* **16** 5233–45
- [78] Wahab O J et al 2023 Proton transport through nanoscale corrugations in two-dimensional crystals *Nature* **620** 782–6
- [79] Bediako D K, Rezaee M, Yoo H, Larson D T, Zhao S Y F, Taniguchi T, Watanabe K, Brower-Thomas T L, Kaxiras E and Kim P 2018 Heterointerface effects in the electrointercalation of van der Waals heterostructures *Nature* **558** 425–9
- [80] Li Y, Lu Y, Adelhelm P, Titirici M-M and Hu Y-S 2019 Intercalation chemistry of graphite: alkali metal ions and beyond *Chem. Soc. Rev.* **48** 4655–87
- [81] Hui J, Burgess M, Zhang J and Rodríguez-López J 2016 Layer number dependence of Li^+ intercalation on few-layer graphene and electrochemical imaging of its solid–electrolyte interphase evolution *ACS Nano* **10** 4248–57
- [82] Barton Z J and Rodríguez-López J 2014 Lithium ion quantification using mercury amalgams as in situ electrochemical probes in nonaqueous media *Anal. Chem.* **86** 10660–7
- [83] Gossage Z T, Hui J, Sarbapalli D and Rodríguez-López J 2020 Coordinated mapping of Li^+ flux and electron transfer reactivity during solid–electrolyte interphase formation at a graphene electrode *Analyst* **145** 2631–8
- [84] Gossage Z T, Hui J, Zeng Y, Flores-Zuleta H and Rodríguez-López J 2019 Probing the reversibility and kinetics of Li^+ during SEI formation and (de)intercalation on edge plane graphite using ion-sensitive scanning electrochemical microscopy *Chem. Sci.* **10** 10749–54
- [85] Zeng Y, Gossage Z T, Sarbapalli D, Hui J and Rodríguez-López J 2022 Tracking passivation and cation flux at incipient solid–electrolyte interphases on multi-layer graphene using high resolution scanning electrochemical microscopy *ChemElectroChem* **9** e202101445
- [86] Sarbapalli D et al 2022 A surface modification strategy towards reversible Na-ion intercalation on graphitic carbon using fluorinated few-layer graphene *J. Electrochem. Soc.* **169** 106522
- [87] Mazánek V, Luxa J, Matějková S, Kučera J, Sedmidubský D, Pumera M and Sofer Z 2019 Ultrapure graphene is a poor electrocatalyst: definitive proof of the key role of metallic impurities in graphene-based electrocatalysis *ACS Nano* **13** 1574–82
- [88] Zhu Y, Peng W, Li Y, Zhang G, Zhang F and Fan X 2019 Multiple roles of a heterointerface in two-dimensional van der Waals heterostructures: insights into energy-related applications *J. Mater. Chem. A* **7** 23577–603
- [89] Bayatsarmadi B, Zheng Y, Vasileff A and Qiao S-Z 2017 Recent advances in atomic metal doping of carbon-based nanomaterials for energy conversion *Small* **13** 1700191

- [90] Sławińska J, Dabrowski P and Zasada I 2011 Doping of graphene by a Au(111) substrate: calculation strategy within the local density approximation and a semiempirical van der Waals approach *Phys. Rev. B* **83** 245429
- [91] Decker R, Wang Y, Brar V W, Regan W, Tsai H-Z, Wu Q, Gannett W, Zettl A and Crommie M F 2011 Local electronic properties of graphene on a BN substrate via scanning tunneling microscopy *Nano Lett.* **11** 2291–5
- [92] Hui J, Pakhira S, Bhargava R, Barton Z J, Zhou X, Chinderle A J, Mendoza-Cortes J L and Rodríguez-López J 2018 Modulating electrocatalysis on graphene heterostructures: physically impermeable yet electronically transparent electrodes *ACS Nano* **12** 2980–90
- [93] Schorr N B, Counihan M J, Bhargava R and Rodríguez-López J 2020 Impact of plasmonic photothermal effects on the reactivity of Au nanoparticle modified graphene electrodes visualized using scanning electrochemical microscopy *Anal. Chem.* **92** 3666–73
- [94] Gong Y, Xu Z-Q, Li D, Zhang J, Aharonovich I and Zhang Y 2021 Two-dimensional hexagonal boron nitride for building next-generation energy-efficient devices *ACS Energy Lett.* **6** 985–96
- [95] Liu D-Q, Tao B, Ruan H-C, Bentley C L and Unwin P R 2019 Metal support effects in electrocatalysis at hexagonal boron nitride *Chem. Commun.* **55** 628–31
- [96] Jiao Y, Zheng Y, Davey K and Qiao S-Z 2016 Activity origin and catalyst design principles for electrocatalytic hydrogen evolution on heteroatom-doped graphene *Nat. Energy* **1** 16130
- [97] Kumatani A et al 2019 Chemical dopants on edge of holey graphene accelerate electrochemical hydrogen evolution reaction *Adv. Sci.* **6** 1900119
- [98] Jin R, Cheng L, Lu H, Zhuang J, Jiang D and Chen H-Y 2021 High spatial resolution electrochemical microscopic observation of enhanced charging under bias at active sites of N-rGO *ACS Appl. Energy Mater.* **4** 3502–7
- [99] Cheng L, Jin R, Jiang D, Zhuang J, Liao X and Zheng Q 2021 Scanning electrochemical cell microscopy platform with local electrochemical impedance spectroscopy *Anal. Chem.* **93** 16401–8
- [100] Dechant A, Ohto T, Ito Y, Makarova M V, Kawabe Y, Agari T, Kumai H, Takahashi Y, Naito H and Kotani M 2021 Geometric model of 3D curved graphene with chemical dopants *Carbon* **182** 223–32
- [101] Bottari G, Herranz M Á, Wibmer L, Volland M, Rodríguez-Pérez L, Guldi D M, Hirsch A, Martín N, D'Souza F and Torres T 2017 Chemical functionalization and characterization of graphene-based materials *Chem. Soc. Rev.* **46** 4464–500
- [102] Georgakilas V, Otyepka M, Bourlinos A B, Chandra V, Kim N, Kemp K C, Hobza P, Zboril R and Kim K S 2012 Functionalization of graphene: covalent and non-covalent approaches, derivatives and applications *Chem. Rev.* **112** 6156–214
- [103] Liu L, Tan C, Chai J, Wu S, Radko A, Zhang H and Mandler D 2014 Electrochemically “writing” graphene from graphene oxide *Small* **10** 3555–9
- [104] Molina J, Fernández J and Cases F 2016 Scanning electrochemical microscopy for the analysis and patterning of graphene materials: a review *Synth. Met.* **222** 145–61
- [105] Ku S-Y, Wong K-T and Bard A J 2008 Surface patterning with fluorescent molecules using click chemistry directed by scanning electrochemical microscopy *J. Am. Chem. Soc.* **130** 2392–3
- [106] Torbensen K, Kongsefelt M, Shimizu K, Pedersen E B, Skrydstrup T, Pedersen S U and Daasbjerg K 2015 Patterned carboxylation of graphene using scanning electrochemical microscopy *Langmuir* **31** 4443–52
- [107] Pham-Truong T-N, Deng B, Liu Z, Randriamahazaka H and Ghilane J 2018 Local electrochemical reactivity of single layer graphene deposited on flexible and transparent plastic film using scanning electrochemical microscopy *Carbon* **130** 566–73
- [108] Rodríguez-López J, Ritzert N L, Mann J A, Tan C, Dichtel W R and Abruña H D 2012 Quantification of the surface diffusion of tripodal binding motifs on graphene using scanning electrochemical microscopy *J. Am. Chem. Soc.* **134** 6224–36
- [109] Pumera M, Sofer Z and Ambrosi A 2014 Layered transition metal dichalcogenides for electrochemical energy generation and storage *J. Mater. Chem. A* **2** 8981–7
- [110] Chia X and Pumera M 2018 Characteristics and performance of two-dimensional materials for electrocatalysis *Nat. Catal.* **1** 909–21
- [111] Velický M et al 2015 Electron transfer kinetics on natural crystals of MoS₂ and graphite *Phys. Chem. Chem. Phys.* **17** 17844–53
- [112] Ritzert N L, Szalai V A and Moffat T P 2018 Mapping electron transfer at MoS₂ using scanning electrochemical microscopy *Langmuir* **34** 13864–70
- [113] Cabré M B, Paiva A E, Velický M, Colavita P E and McKelvey K 2022 Electrochemical detection of isolated nanoscale defects in 2D transition metal dichalcogenides *J. Phys. Chem. C* **126** 11636–41
- [114] Voiry D, Salehi M, Silva R, Fujita T, Chen M, Asefa T, Shenoy V B, Eda G and Chhowalla M 2013 Conducting MoS₂ nanosheets as catalysts for hydrogen evolution reaction *Nano Lett.* **13** 6222–7
- [115] Bo T, Wang X, Jia R, Han L, Xin H L, Zhang H, Miller E M and Mirkin M V 2021 Probing activities of individual catalytic nanoflakes by tunneling mode of scanning electrochemical microscopy *J. Phys. Chem. C* **125** 25525–32
- [116] Sun T, Zhang H, Wang X, Liu J, Xiao C, Nanayakkara S U, Blackburn J L, Mirkin M V and Miller E M 2019 Nanoscale mapping of hydrogen evolution on metallic and semiconducting MoS₂ nanosheets *Nanoscale Horiz.* **4** 619–24
- [117] Zhang H, Koledin T D, Wang X, Hao J, Nanayakkara S U, Attanayake N H, Li Z, Mirkin M V and Miller E M 2022 Stabilizing the heavily-doped and metallic phase of MoS₂ monolayers with surface functionalization *2D Mater.* **9** 015033
- [118] Brunet Cabré M, Paiva A E, Velický M, Colavita P E and McKelvey K 2021 Electrochemical kinetics as a function of transition metal dichalcogenide thickness *Electrochim. Acta* **393** 139027
- [119] Du H-Y, Huang Y-F, Wong D, Tseng M-F, Lee Y-H, Wang C-H, Lin C-L, Hoffmann G, Chen K-H and Chen L-C 2021 Nanoscale redox mapping at the MoS₂-liquid interface *Nat. Commun.* **12** 1321
- [120] Maroo S, Yu Y, Taniguchi T, Watanabe K and Bediako D K 2023 Decoupling effects of electrostatic gating on electronic transport and interfacial charge-transfer kinetics at few-layer molybdenum disulfide *ACS Nanosci. Au* **3** 204–10
- [121] Mondal A and Vomiero A 2022 2D transition metal dichalcogenides-based electrocatalysts for hydrogen evolution reaction *Adv. Funct. Mater.* **32** 2208994
- [122] Schmickler W and Santos E 2010 *Interfacial Electrochemistry* 2nd edn (Springer)
- [123] Chen Y, Yang K, Jiang B, Li J, Zeng M and Fu L 2017 Emerging two-dimensional nanomaterials for electrochemical hydrogen evolution *J. Mater. Chem. A* **5** 8187–208
- [124] Hinnemann B, Moses P G, Bonde J, Jørgensen K P, Nielsen J H, Horch S, Chorkendorff I and Nørskov J K 2005 Biomimetic hydrogen evolution: MoS₂ nanoparticles as catalyst for hydrogen evolution *J. Am. Chem. Soc.* **127** 5308–9
- [125] Jaramillo T F, Jørgensen K P, Bonde J, Nielsen J H, Horch S and Chorkendorff I 2007 Identification of active edge sites for electrochemical H₂ evolution from MoS₂ nanocatalysts *Science* **317** 100–2
- [126] Bentley C L, Kang M, Maddar F M, Li F, Walker M, Zhang J and Unwin P R 2017 Electrochemical maps and movies of the hydrogen evolution reaction on natural crystals of

- molybdenite (MoS₂): basal vs. edge plane activity *Chem. Sci.* **8** 6583–93
- [127] Daviddi E, Gonos K L, Colburn A W, Bentley C L and Unwin P R 2019 Scanning electrochemical cell microscopy (SECCM) chronopotentiometry: development and applications in electroanalysis and electrocatalysis *Anal. Chem.* **91** 9229–37
- [128] Tao B, Unwin P R and Bentley C L 2020 Nanoscale variations in the electrocatalytic activity of layered transition-metal dichalcogenides *J. Phys. Chem. C* **124** 789–98
- [129] Ye G, Gong Y, Lin J, Li B, He Y, Pantelides S T, Zhou W, Vajtai R and Ajayan P M 2016 Defects engineered monolayer MoS₂ for improved hydrogen evolution reaction *Nano Lett.* **16** 1097–103
- [130] Tsai C, Li H, Park S, Park J, Han H S, Nørskov J K, Zheng X and Abild-Pedersen F 2017 Electrochemical generation of sulfur vacancies in the basal plane of MoS₂ for hydrogen evolution *Nat. Commun.* **8** 15113
- [131] Takahashi Y et al 2020 High-resolution electrochemical mapping of the hydrogen evolution reaction on transition-metal dichalcogenide nanosheets *Angew. Chem., Int. Ed.* **59** 3601–8
- [132] Li H et al 2016 Activating and optimizing MoS₂ basal planes for hydrogen evolution through the formation of strained sulphur vacancies *Nat. Mater.* **15** 48–53
- [133] Li H, Du M, Mleczko M J, Koh A L, Nishi Y, Pop E, Bard A J and Zheng X 2016 Kinetic study of hydrogen evolution reaction over strained MoS₂ with sulfur vacancies using scanning electrochemical microscopy *J. Am. Chem. Soc.* **138** 5123–9
- [134] Jasion D, Barforoush J M, Qiao Q, Zhu Y, Ren S and Leonard K C 2015 Low-dimensional hyperthin FeS₂ nanostructures for efficient and stable hydrogen evolution electrocatalysis *ACS Catal.* **5** 6653–7
- [135] Splendiani A, Sun L, Zhang Y, Li T, Kim J, Chim C-Y, Galli G and Wang F 2010 Emerging photoluminescence in monolayer MoS₂ *Nano Lett.* **10** 1271–5
- [136] Velický M, Bissett M A, Woods C R, Toth P S, Georgiou T, Kinloch I A, Novoselov K S and Dryfe R A W 2016 Photoelectrochemistry of pristine mono- and few-layer MoS₂ *Nano Lett.* **16** 2023–32
- [137] Yu X, Guijarro N, Johnson M and Sivula K 2018 Defect mitigation of solution-processed 2D WSe₂ nanoflakes for solar-to-hydrogen conversion *Nano Lett.* **18** 215–22
- [138] Wang L, Tahir M, Chen H and Sambur J B 2019 Probing charge carrier transport and recombination pathways in monolayer MoS₂/WS₂ heterojunction photoelectrodes *Nano Lett.* **19** 9084–94
- [139] Isenberg A E, Todt M A, Wang L and Sambur J B 2018 Role of photogenerated iodine on the energy-conversion properties of MoSe₂ nanoflake liquid junction photovoltaics *ACS Appl. Mater. Interfaces* **10** 27780–6
- [140] Todt M A, Isenberg A E, Nanayakkara S U, Miller E M and Sambur J B 2018 Single-nanoflake photo-electrochemistry reveals champion and spectator flakes in exfoliated MoSe₂ films *J. Phys. Chem. C* **122** 6539–45
- [141] Hill J W and Hill C M 2019 Directly mapping photoelectrochemical behavior within individual transition metal dichalcogenide nanosheets *Nano Lett.* **19** 5710–6
- [142] Velazquez J M et al 2016 A scanning probe investigation of the role of surface motifs in the behavior of p-WSe₂ photocathodes *Energy Environ. Sci.* **9** 164–75
- [143] Hill J W, Fu Z, Tian J and Hill C M 2020 Locally engineering and interrogating the photoelectrochemical behavior of defects in transition metal dichalcogenides *J. Phys. Chem. C* **124** 17141–9
- [144] Strange L E, Yadav J, Garg S, Shinde P S, Hill J W, Hill C M, Kung P and Pan S 2020 Investigating the redox properties of two-dimensional MoS₂ using photoluminescence spectroelectrochemistry and scanning electrochemical cell microscopy *J. Phys. Chem. Lett.* **11** 3488–94
- [145] Hill J W and Hill C M 2021 Directly visualizing carrier transport and recombination at individual defects within 2D semiconductors *Chem. Sci.* **12** 5102–12
- [146] Tolbert Chloe C and Hill C M 2022 Electrochemically probing exciton transport in monolayers of two-dimensional semiconductors *Faraday Discuss.* **233** 163–74
- [147] Fu Z, Hill J W, Parkinson B, Hill C M and Tian J 2022 Layer and material-type dependent photoresponse in WSe₂/WS₂ vertical heterostructures *2D Mater.* **9** 015022
- [148] Lee C-H et al 2014 Atomically thin p–n junctions with van der Waals heterointerfaces *Nat. Nanotechnol.* **9** 676–81
- [149] Zheng H, Li M, Chen J, Quan A, Ye K, Ren H, Hu S and Cao Y 2022 Strain tuned efficient heterostructure photoelectrodes *Chin. Chem. Lett.* **33** 1450–4
- [150] Liu Y, Jin C, Liu Y, Ruiz K H, Ren H, Fan Y, White H S and Chen Q 2021 Visualization and quantification of electrochemical H₂ bubble nucleation at Pt, Au, and MoS₂ substrates *ACS Sens.* **6** 355–63
- [151] Liu Y, Lu X, Peng Y and Chen Q 2021 Electrochemical visualization of gas bubbles on superaerophobic electrodes using scanning electrochemical cell microscopy *Anal. Chem.* **93** 12337–45
- [152] Trotochaud L, Ranney J K, Williams K N and Boettcher S W 2012 Solution-cast metal oxide thin film electrocatalysts for oxygen evolution *J. Am. Chem. Soc.* **134** 17253–61
- [153] Subbaraman R, Tripkovic D, Chang K-C, Strmcnik D, Paulikas A P, Hirunsit P, Chan M, Greeley J, Stamenkovic V and Markovic N M 2012 Trends in activity for the water electrolyser reactions on 3d M(Ni,Co,Fe,Mn) hydr(oxy)oxide catalysts *Nat. Mater.* **11** 550–7
- [154] Zhao Y, Jia X, Chen G, Shang L, Waterhouse G I N, Wu L-Z, Tung C-H, O'Hare D and Zhang T 2016 Ultrafine NiO nanosheets stabilized by TiO₂ from monolayer NiTi-LDH precursors: an active water oxidation electrocatalyst *J. Am. Chem. Soc.* **138** 6517–24
- [155] Sun T, Wang D, Mirkin M V, Cheng H, Zheng J-C, Richards R M, Lin F and Xin H L 2019 Direct high-resolution mapping of electrocatalytic activity of semi-two-dimensional catalysts with single-edge sensitivity *Proc. Natl Acad. Sci. USA* **116** 11618–23
- [156] Mefford J T et al 2021 Correlative operando microscopy of oxygen evolution electrocatalysts *Nature* **593** 67–73
- [157] Hong Ng V M, Huang H, Zhou K, Lee P S, Que W, Xu J Z and Kong L B 2017 Recent progress in layered transition metal carbides and/or nitrides (MXenes) and their composites: synthesis and applications *J. Mater. Chem. A* **5** 3039–68
- [158] Anasori B, Lukatskaya M R and Gogotsi Y 2017 2D metal carbides and nitrides (MXenes) for energy storage *Nat. Rev. Mater.* **2** 16098
- [159] Hantanasirisakul K and Gogotsi Y 2018 Electronic and optical properties of 2D transition metal carbides and nitrides (MXenes) *Adv. Mater.* **30** 1804779
- [160] Gupta S, Ringo W, Hu M and Wang X 2020 Two-dimensional titanium carbide (Ti₃C₂T_x) MXenes of different flake sizes studied by scanning electrochemical microscopy in different electrolytes *J. Electron. Mater.* **49** 4028–44
- [161] Djire A, Wang X, Xiao C, Nwamba O C, Mirkin M V and Neale N R 2020 Basal plane hydrogen evolution activity from mixed metal nitride MXenes measured by scanning electrochemical microscopy *Adv. Funct. Mater.* **30** 2001136
- [162] Spencer M A, Fortunato J and Augustyn V 2022 Electrochemical proton insertion modulates the hydrogen evolution reaction on tungsten oxides *J. Chem. Phys.* **156** 064704
- [163] Brunet Cabré M, Spurling D, Martinuz P, Longhi M, Schröder C, Nolan H, Nicolosi V, Colavita P E and McKelvey K 2023 Isolation of pseudocapacitive surface processes at monolayer MXene flakes reveals delocalized charging mechanism *Nat. Commun.* **14** 374

- [164] Jiang Z, Zhou W, Hong A, Guo M, Luo X and Yuan C 2019 MoS₂ moiré superlattice for hydrogen evolution reaction *ACS Energy Lett.* **4** 2830–5
- [165] Haid R W, Kluge R M, Liang Y and Bandarenka A S 2021 In situ quantification of the local electrocatalytic activity via electrochemical scanning tunneling microscopy *Small Methods* **5** 2000710
- [166] Zhang Z, Said S, Smith K, Jervis R, Howard C A, Shearing P R, Brett D J L and Miller T S 2021 Characterizing batteries by in situ electrochemical atomic force microscopy: a critical review *Adv. Energy Mater.* **11** 2101518
- [167] Bae J H, Yu Y and Mirkin M V 2017 Diffuse layer effect on electron-transfer kinetics measured by scanning electrochemical microscopy (SECM) *J. Phys. Chem. Lett.* **8** 1338–42
- [168] Lim K, Goines S, Deng M, McCormick H, Kauffmann P J and Dick J E 2023 A troubleshooting guide for laser pulling platinum nanoelectrodes *Analyst* **148** 2992–3001
- [169] Lin Y-H, Tsai C-N, Chen P-F, Lin Y-T, Darvishi S, Girault H H, Lin T-Y, Liao M-Y and Lin T-E 2022 AI-assisted fusion of scanning electrochemical microscopy images using novel soft probe *ACS Meas. Sci. Au* **2** 576–83
- [170] Stephens L I, Payne N A and Mauzeroll J 2020 Super-resolution scanning electrochemical microscopy *Anal. Chem.* **92** 3958–63
- [171] Anupriya E S and Shen M 2022 New method in surface treatment of nanopipette for interface between two immiscible electrolyte solutions (ITIES) experiment *J. Electrochem. Soc.* **169** 046501
- [172] Li Y, Morel A, Gallant D and Mauzeroll J 2020 Oil-immersed scanning micropipette contact method enabling long-term corrosion mapping *Anal. Chem.* **92** 12415–22
- [173] Martín-Yerga D, Kang M and Unwin P R 2021 Scanning electrochemical cell microscopy in a glovebox: structure-activity correlations in the early stages of solid-electrolyte interphase formation on graphite *ChemElectroChem* **8** 4240–51
- [174] Momotenko D, Byers J C, McKelvey K, Kang M and Unwin P R 2015 High-speed electrochemical imaging *ACS Nano* **9** 8942–52
- [175] Kuss S, Trinh D, Danis L and Mauzeroll J 2015 High-speed scanning electrochemical microscopy method for substrate kinetic determination: method and theory *Anal. Chem.* **87** 8096–101
- [176] Kandel S, Zhou T, Babu A V, Di Z, Li X, Ma X, Holt M, Miceli A, Phatak C and Cherukara M J 2023 Demonstration of an AI-driven workflow for autonomous high-resolution scanning microscopy *Nat. Commun.* **14** 5501
- [177] Sotres J, Boyd H and Gonzalez-Martinez J F 2021 Enabling autonomous scanning probe microscopy imaging of single molecules with deep learning *Nanoscale* **13** 9193–203
- [178] Martín-Yerga D, Unwin P R, Valavanis D and Xu X 2023 Correlative co-located electrochemical multi-microscopy *Curr. Opin. Electrochem.* **42** 101405
- [179] Lu J, Hua X and Long Y-T 2017 Recent advances in real-time and in situ analysis of an electrode–electrolyte interface by mass spectrometry *Analyst* **142** 691–9
- [180] Mao S, Chang J, Pu H, Lu G, He Q, Zhang H and Chen J 2017 Two-dimensional nanomaterial-based field-effect transistors for chemical and biological sensing *Chem. Soc. Rev.* **46** 6872–904
- [181] Lukowski M A, Daniel A S, Meng F, Forticaux A, Li L and Jin S 2013 Enhanced hydrogen evolution catalysis from chemically exfoliated metallic MoS₂ nanosheets *J. Am. Chem. Soc.* **135** 10274–7
- [182] Wu L, Dzade N Y, Yu M, Mezari B, van Hoof A J E, Friedrich H, de Leeuw N H, Hensen E J M and Hofmann J P 2019 Unraveling the role of lithium in enhancing the hydrogen evolution activity of MoS₂: intercalation versus adsorption *ACS Energy Lett.* **4** 1733–40
- [183] Wang J, Yan M, Zhao K, Liao X, Wang P, Pan X, Yang W and Mai L 2017 Field effect enhanced hydrogen evolution reaction of MoS₂ nanosheets *Adv. Mater.* **29** 1604464
- [184] Wang Y, Udyavara S, Neurock M and Frisbie C D 2019 Field effect modulation of electrocatalytic hydrogen evolution at back-gated two-dimensional MoS₂ electrodes *Nano Lett.* **19** 6118–23
- [185] Yan M et al 2017 Field-effect tuned adsorption dynamics of VSe₂ nanosheets for enhanced hydrogen evolution reaction *Nano Lett.* **17** 4109–15
- [186] Iannaccone G, Bonaccorso F, Colombo L and Fiori G 2018 Quantum engineering of transistors based on 2D materials heterostructures *Nat. Nanotechnol.* **13** 183–91
- [187] Wang L, Chen W, Zhang D, Du Y, Amal R, Qiao S, Wu J and Yin Z 2019 Surface strategies for catalytic CO₂ reduction: from two-dimensional materials to nanoclusters to single atoms *Chem. Soc. Rev.* **48** 5310–49
- [188] Hasani A, Tekalgne M, Le Q V, Jang H W and Kim S Y 2019 Two-dimensional materials as catalysts for solar fuels: hydrogen evolution reaction and CO₂ reduction *J. Mater. Chem. A* **7** 430–54
- [189] Zhao J and Chen Z 2017 Single Mo atom supported on defective boron nitride monolayer as an efficient electrocatalyst for nitrogen fixation: a computational study *J. Am. Chem. Soc.* **139** 12480–7
- [190] Kai T, Zhou M, Duan Z, Henkelman G A and Bard A J 2017 Detection of CO₂^{•-} in the electrochemical reduction of carbon dioxide in N,N-dimethylformamide by scanning electrochemical microscopy *J. Am. Chem. Soc.* **139** 18552–7
- [191] Zhou M, Yu Y, Hu K and Mirkin M V 2015 Nanoelectrochemical approach to detecting short-lived intermediates of electrocatalytic oxygen reduction *J. Am. Chem. Soc.* **137** 6517–23
- [192] Wert S, Iffelsberger C, Novčić K A and Pumera M 2022 Corrosion of catalyst in high resolution: layered transition metal dichalcogenides electrocatalyse water splitting and corrode during the process *J. Catal.* **416** 85–91
- [193] Mu H, Yu W, Yuan J, Lin S and Zhang G 2022 Interface and surface engineering of black phosphorus: a review for optoelectronic and photonic applications *Mater. Futures* **1** 012301
- [194] Liu H, Hu K, Yan D, Chen R, Zou Y, Liu H and Wang S 2018 Recent advances on black phosphorus for energy storage, catalysis, and sensor applications *Adv. Mater.* **30** 1800295
- [195] Jiao L and Jiang H-L 2019 Metal-organic-framework-based single-atom catalysts for energy applications *Chem* **5** 786–804
- [196] Novoselov K S, Mishchenko A, Carvalho A and Castro Neto A H 2016 2D materials and van der Waals heterostructures *Science* **353** aac9439
- [197] Geim A K and Grigorieva I V 2013 Van der Waals heterostructures *Nature* **499** 419–25
- [198] Zhuang R et al 2023 Solution-grown BiI/BiI₃ van der Waals heterostructures for sensitive x-ray detection *Nat. Commun.* **14** 1621
- [199] Su Z, Zhao Y, Huang Y, Xu C, Yang X, Wang B, Xu B, Xu S and Bai G 2023 Light-driven soft actuator based on graphene and WSe₂ nanosheets composite for multimodal motion and remote manipulation *Nano Res.* **16** 1313–9
- [200] Morkvenaite-Vilkonciene I, Ramanaviciene A, Kisieliute A, Bucinskas V and Ramanavicius A 2019 Scanning electrochemical microscopy in the development of enzymatic sensors and immunosensors *Biosens. Bioelectron.* **141** 111411
- [201] Maciejewska M, Schäfer D and Schuhmann W 2006 SECM imaging of spatial variability in biosensor architectures *Electrochem. Commun.* **8** 1119–24
- [202] Sulleiro M V, Dominguez-Alfaro A, Alegret N, Silvestri A and Gómez I J 2022 2D materials towards sensing technology: from fundamentals to applications *Sens. Bio-Sens. Res.* **38** 100540
- [203] Strange L E, Li X, Wornyo E, Ashaduzzaman M and Pan S 2023 Scanning electrochemical microscopy for chemical

- imaging and understanding redox activities of battery materials *Chem. Biomed. Imaging* **1** 110–20
- [204] Ventosa E and Schuhmann W 2015 Scanning electrochemical microscopy of Li-ion batteries *Phys. Chem. Chem. Phys.* **17** 28441–50
- [205] Wang J, Malgras V, Sugahara Y and Yamauchi Y 2021 Electrochemical energy storage performance of 2D nanoarchitected hybrid materials *Nat. Commun.* **12** 3563
- [206] Wu M, Zheng W, Hu X, Zhan F, He Q, Wang H, Zhang Q and Chen L 2022 Exploring 2D energy storage materials: advances in structure, synthesis, optimization strategies, and applications for monovalent and multivalent metal-ion hybrid capacitors *Small* **18** 2205101